Article

Cell Stem Cell

Efficient Derivation of Functional Human Airway Epithelium from Pluripotent Stem Cells via Temporal Regulation of Wnt Signaling

Graphical Abstract

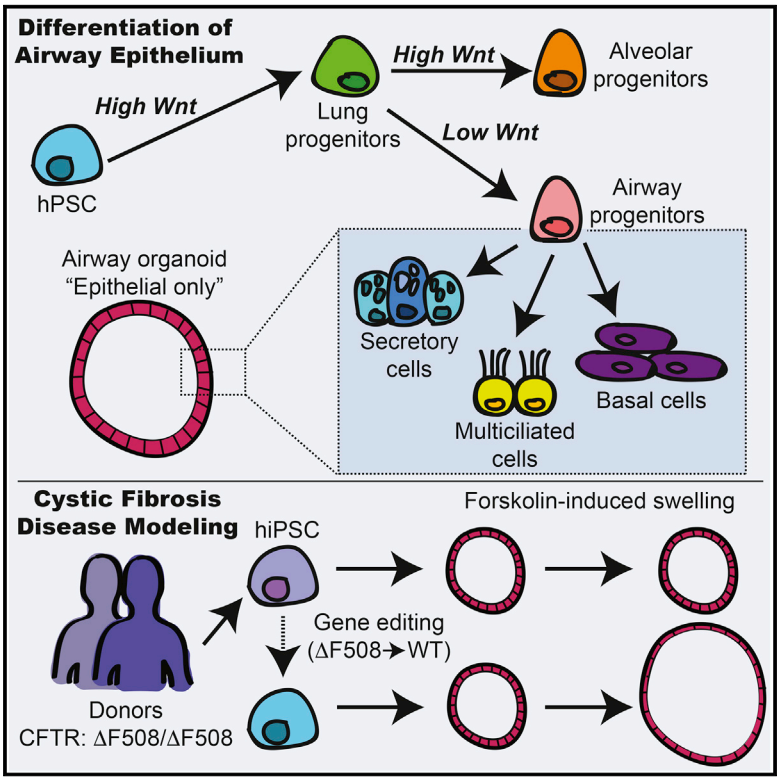

Highlights

- Wnt signaling regulates lung differentiation of human pluripotent stem cells
- Withdrawal of Wnt signaling from lung progenitors prompts rapid proximal patterning
- Purified lung progenitors differentiate to airway organoids in low Wnt conditions
- Derived organoids exhibit CFTR-dependent swelling in response to forskolin

Authors

Katherine B. McCauley, Finn Hawkins, Maria Serra, Dylan C. Thomas, Anjali Jacob, Darrell N. Kotton

Correspondence

dkotton@bu.edu

In Brief

Kotton and colleagues show that carefully timed regulation of Wnt signaling can direct human pluripotent cells to differentiate rapidly into functional airway epithelial organoids with many potential applications in disease modeling, drug screening, and precision medicine, and for diseases such as cystic fibrosis.

McCauley et al., 2017, Cell Stem Cell *20*, 1–14
June 1, 2017
http://dx.doi.org/10.1016/j.stem.2017.03.001

CellPress

Please cite this article in press as: McCauley et al., Efficient Derivation of Functional Human Airway Epithelium from Pluripotent Stem Cells via Temporal Regulation of Wnt Signaling, Cell Stem Cell (2017), http://dx.doi.org/10.1016/j.stem.2017.03.001

Cell Stem Cell
Article

Efficient Derivation of Functional Human Airway Epithelium from Pluripotent Stem Cells via Temporal Regulation of Wnt Signaling

Katherine B. McCauley,[1,2] Finn Hawkins,[1,2] Maria Serra,[1,2] Dylan C. Thomas,[1] Anjali Jacob,[1,2] and Darrell N. Kotton[1,2,3,*]
[1]Center for Regenerative Medicine of Boston University and Boston Medical Center, Boston, MA 02118, USA
[2]The Pulmonary Center and Department of Medicine, Boston University School of Medicine, Boston, MA 02118, USA
[3]Lead Contact
*Correspondence: dkotton@bu.edu
http://dx.doi.org/10.1016/j.stem.2017.03.001

SUMMARY

Effective derivation of functional airway organoids from induced pluripotent stem cells (iPSCs) would provide valuable models of lung disease and facilitate precision therapies for airway disorders such as cystic fibrosis. However, limited understanding of human airway patterning has made this goal challenging. Here, we show that cyclical modulation of the canonical Wnt signaling pathway enables rapid directed differentiation of human iPSCs via an NKX2-1$^+$ progenitor intermediate into functional proximal airway organoids. We find that human NKX2-1$^+$ progenitors have high levels of Wnt activation but respond intrinsically to decreases in Wnt signaling by rapidly patterning into proximal airway lineages at the expense of distal fates. Using this directed approach, we were able to generate cystic fibrosis patient-specific iPSC-derived airway organoids with a defect in forskolin-induced swelling that is rescued by gene editing to correct the disease mutation. Our approach has many potential applications in modeling and drug screening for airway diseases.

INTRODUCTION

Directed differentiation of functional lung epithelial cell types from human pluripotent stem cells (PSCs) holds promise for in vitro modeling of complex respiratory diseases and for future cell-based regenerative therapies. Recent studies, including our own, have demonstrated that a heterogeneous mixture of diverse lung epithelia accompanied by non-lung lineages can be simultaneously "co-derived" from PSCs differentiated in vitro for several weeks or months (Dye et al., 2015; Firth et al., 2014; Gotoh et al., 2014; Green et al., 2011; Huang et al., 2014; Konishi et al., 2016; Longmire et al., 2012; Mou et al., 2012; Wong et al., 2012). However, many pulmonary diseases, such as cystic fibrosis, have their primary effects within distinct regions of the lungs and their constituent cellular subtypes. The heterogeneity of current differentiation outcomes therefore potentially hampers attempts to apply these PSC-based models to recapitulate pulmonary disease and test therapies in vitro. While recent cell sorting methods have enabled the derivation of more homogeneous populations of lung epithelial progenitor cells or their differentiated progeny from human PSCs (hPSCs) (Gotoh et al., 2014; Hawkins et al., 2017; Konishi et al., 2016), the consistent derivation of well-defined, mature functional lineages from these progenitors for effective disease modeling has remained challenging, due in part to heterogeneous or stochastic differentiation in protocols that can depend on many weeks or months of cell culture.

One approach to realize the promise of hPSC model systems for studying diseases affecting specific cellular subtypes is to engineer in vitro methods that more closely mimic in vivo developmental cell fate decisions. In contrast to current prolonged in vitro approaches, in vivo lung development is a tightly controlled process, where chaotic heterogeneity is minimized by signaling cascades that act cyclically in a regiospecific manner during narrow stage-dependent windows of time to precisely and rapidly promote appropriate cell fates while suppressing alternate fate options. The patterning of early lung epithelial progenitors in vivo in mouse embryos is a classic example of this phenomenon, because soon after lineage specification of primordial lung epithelial progenitors, indicated by emergence of Nkx2-1$^+$ endoderm, their descendants located at advancing distal lung bud tips are faced with the fate option of either maintaining a distal progenitor phenotype or surrendering this fate as they move away from this distal niche to assume a proximal airway cell fate (Rawlins et al., 2009). Through these fate decisions, the branching lung airways are patterned post-specification along a proximodistal axis, which is canonically defined by the expression of key transcription factors Sox2 in the proximal developing airway and tracheal epithelium and Sox9 in the budding distal tips (Hashimoto et al., 2012; Liu and Hogan, 2002). Because this precise spatiotemporal segregation of Sox2 and Sox9 as canonical proximal and distal lung markers, respectively, has been described in developing mouse lungs it remains somewhat unclear whether these markers may be similarly used as equally faithful proximal-distal epithelial patterning markers in early human lung development. However, recent studies have demonstrated low levels of SOX2 in the human distal lung and high levels in the proximal airways (Kim et al., 2016; Xu et al., 2016), and a variety of additional markers of proximal and distal epithelial differentiation in humans is emerging in

single-cell RNA sequencing studies (Xu et al., 2016) to facilitate the study of airway patterning in early human development.

Recreating the tightly controlled proximodistal patterning of lung cells during in vitro differentiation of iPSC-derived NKX2-1$^+$ progenitors has been difficult in part due to the plethora of developmental signaling pathways that have been described in mouse models as being important to this process, including Wnt, FGF, BMP, TGFβ, RA, SHH, and Notch signaling (Bellusci et al., 1997; Cardoso et al., 1997; Chen et al., 2007, 2010; Hashimoto et al., 2012; Hyatt et al., 2004; Mucenski et al., 2003; Sekine et al., 1999; Shu et al., 2005; Weaver et al., 1999, 2000; Zemke et al., 2009). In particular, it has been noted that these pathways exhibit high levels of temporal and regional specificity by which they each promote the migration, differentiation, and maturation of specific cell types at the expense of others.

Here, we develop an approach for modulating the cell fate decisions of hPSC-derived primordial lung progenitors in a manner that recapitulates in vivo development, resulting in the synchronized modulation of proximal airway versus distal alveolar epithelial patterning. Our method significantly differs from prior attempts (Konishi et al., 2016) by inducing rapid airway differentiation in response to changes in canonical developmental signaling pathways that act intrinsically on lung progenitors. As predicted by in vivo mouse genetic models, in human PSC lung developmental model systems we find the Wnt signaling pathway to be an over-arching regulator of proximodistal epithelial patterning. Withdrawal of Wnt activation promotes swift emergence of proximal over distal epithelial fates from primordial NKX2-1$^+$ progenitors, whereas maintenance of Wnt signaling promotes distal epithelial fates while suppressing proximal fates. The end result of this approach is the reliable production of "epithelial-only" airway organoids that derive directly from NKX2-1$^+$ precursors and contain diverse airway epithelial cell types. Furthermore, when generated from cystic fibrosis patient-specific iPSC lines, either before or after gene editing to correct the CFTR genetic lesion responsible for the disease, these organoids allow precise interrogation of mutant versus corrected CFTR function through forskolin-induced epithelial sphere swelling assays. This human developmental model system thus facilitates disease modeling and drug screening for a variety of genetic diseases affecting the airway epithelium, exemplified by cystic fibrosis.

RESULTS

Screening Developmental Signaling Pathways Reveals Contribution from Wnt and BMP Signaling to Proximodistal Patterning of hPSC-Derived Lung Epithelium

To screen for potential mechanisms regulating human lung epithelial patterning after lung lineage specification, we sought to employ an in vitro lung development model system that uses sequential media in a stepwise, stage-specific approach to recapitulate the lineage specification of relatively undifferentiated (primordial) FOXA2$^+$NKX2-1$^+$ endodermal lung progenitors via anterior foregut endoderm from mouse or human PSCs (Figures 1A and S1A) (Hawkins et al., 2017; Huang et al., 2014, 2015; Longmire et al., 2012). Using this approach, we derived NKX2-1$^+$ lung epithelial progenitors at varying efficiencies from several hPSC lines, including RUES2 (untargeted) and an iPSC line (hereafter C17) carrying a GFP reporter targeted to *NKX2-1*, the first gene locus activated in developing endoderm at the time of lung lineage specification (hereafter NKX2-1^{GFP}, Figures 1B and S1B) (Hawkins et al., 2017). Using these lines, we found that differentiated lung progenitors were enriched for NKX2-1 and FOXA2 expression (Figure S1C) and did not express appreciable markers of other NKX2-1$^+$ lineages (thyroid, *PAX8*; neural, *OLIG2*) in comparison to neuroectodermal and thyroid controls (Figure S1C). Nearly 100% of NKX2-1^{GFP+} cells were EPCAM$^+$ (Figure S1D) and did not express markers of other non-endodermal lineages including PDGFRα, CD31, and CD45 (Figure S1E).

Although these NKX2-1^{GFP+} progenitors are initially undifferentiated or primordial at the time of their emergence in culture (days 9–15) (Hawkins et al., 2017) further time in culture in media supplemented with CHIR99021, FGF10, and KGF results in their differentiation into a heterogeneous population of cells expressing markers consistent with multiple lung lineages characteristic of both proximal airway and distal alveolar epithelia, including *SOX2*, *SOX9*, *TP63*, *SFTPB*, *CFTR*, *SFTPC*, *FOXJ1*, and *SCGB3A2* (Hawkins et al., 2017).

To test whether we could efficiently induce a proximal versus distal program in iPSC-derived lung progenitors, we modulated key developmental pathways beginning on day 15 of differentiation in our model system (Figures 1C–1E), and we monitored changes in *SOX2* and *SOX9* expression that might suggest coordinated proximal versus distal patterning changes in purified NKX2-1^{GFP+} cells within 4 days of treatment. At day 15, post-lung specification, we cultured cells in a base media of "low dose" (10 ng/mL) FGF10 to promote proliferation without strongly inducing patterning (Volckaert et al., 2013). From this base media, we stimulated the following pathways: Wnt signaling via the potent GSK3β inhibitor CHIR99021, hereafter CHIR; FGF signaling using FGF2 or high dose (100 ng/mL) FGF10; BMP signaling using BMP4; and TGFβ signaling using TGFβ1.

We found that conditions containing CHIR resulted in significantly decreased *SOX2* and increased *SOX9* expression in sorted NKX2-1^{GFP+} cells, suggesting abrogated proximal and increased distal patterning within 4 days (day 19; Figure 1E). Suppression of proximal cell fate by CHIR was further supported by decreased expression of the highly specific proximal lung epithelial marker, *SCGB3A2*. BMP signaling activation also suppressed *SOX2* and *SCGB3A2* expression while permitting *SOX9* expression, although to a lesser extent than Wnt activation. Inhibition of BMP signaling with the SMAD1/5/8 inhibitor, dorsomorphin, significantly blocked CHIR-induced distal patterning (CHIR versus CHIR+Dorso $p = 1 \times 10^{-6}$). Addition of the Wnt inhibitor, XAV939, had no effect in conditions without CHIR (data not shown), suggesting low basal Wnt signaling. High dose FGF10 resulted in smaller but statistically significant increased *SOX9* expression (Figure 1E). Concordantly, treatment with escalating doses of FGF10 together with CHIR resulted in additionally increased distal (*SOX9*) and decreased proximal (*SOX2*) patterning (Figure S1F). In contrast, we found that TGFβ signaling had no significant effect on patterning markers (Figure S1G). Finally, to ensure the proximalization pattern was not reliant on FGF stimulation, we compared stimulation with versus

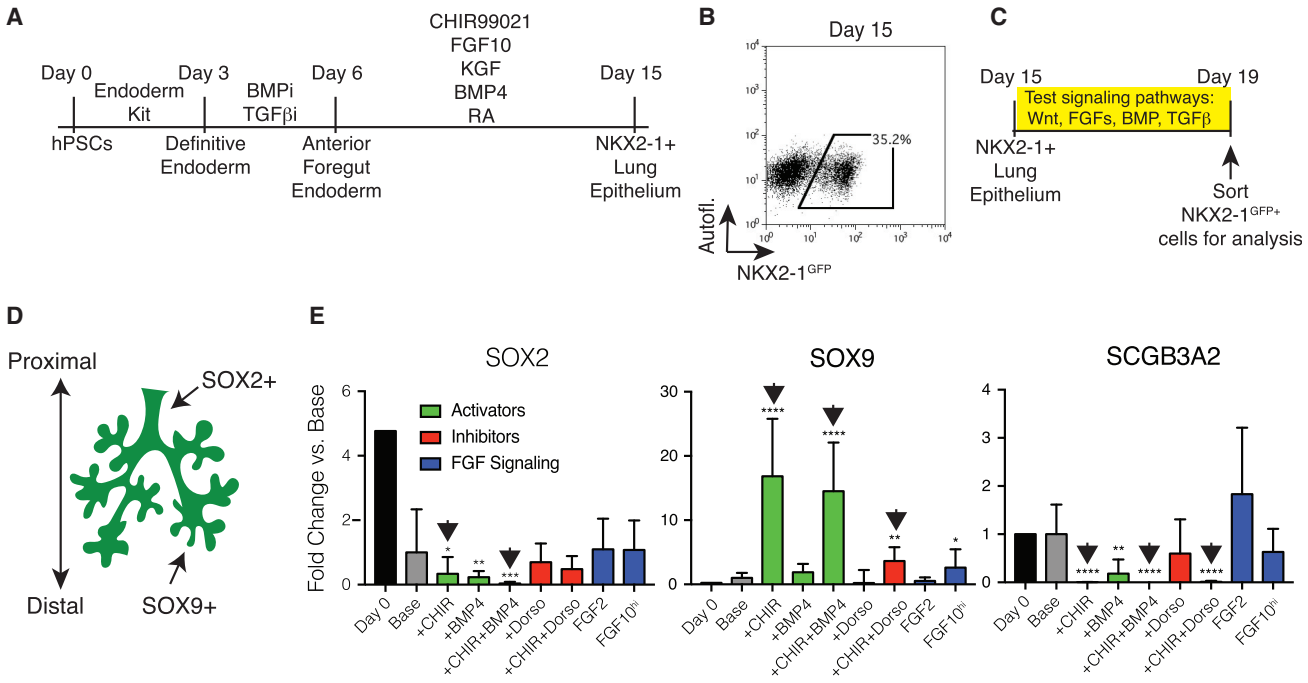

Figure 1. Wnt and BMP4 Signaling Contribute to Proximodistal Pattering of hPSC-Derived Lung Progenitors

(A) Schematic of directed differentiation protocol from hPSCs to NKX2-1^{+} endodermal lung progenitors.

(B) Representative day 15 FACS plot showing typical NKX2-1^{GFP} expression in C17 cells.

(C) Experimental approach for testing developmental pathways. BMPi, BMP inhibition using dorsomorphin; TGFβi, TGFβ inhibition using SB431542.

(D) Schematic of murine branching lung depicting key proximodistal patterning markers.

(E) qRT-PCR measurement of fold change ($2^{-\Delta\Delta Ct}$) of mRNA expression (compared to day 19 base media) shown for day 0 iPSCs or NKX2-1^{GFP+}-sorted cells on day 19 after treatment with indicated growth factors from day 15 to day 19. Base media (day 19 control condition without supplements) is defined as fold change = 1. Arrows indicate conditions containing CHIR99021. Bars represent mean ± SD (Base, +CHIR: n = 6; others: n = 3 biological replicates of independent wells of a differentiation) *p ≤ 0.05, **p ≤ 0.01, ***p ≤ 0.001, ****p ≤ 0.0001 by unpaired two-tailed Student's t test between test conditions and base.

See also Figure S1.

without CHIR added to media alone (without addition of any FGF ligands) and found increased expression of *SCGB3A2* in unsorted cells in the no CHIR condition (data not shown).

Taken together, this initial signaling pathway screen suggested that hPSC-derived lung epithelium responds within 4 days to signaling cues, and Wnt activation via CHIR potentially maintains distal over proximal epithelial patterning early post-lung specification. These patterning changes in human cells are consistent with prior mouse genetic studies suggesting modulation of Wnt activity impacts lung proximodistal patterning during development (De Langhe et al., 2005; Hashimoto et al., 2012; Mucenski et al., 2003; Ramasamy et al., 2007; Shu et al., 2005; Volckaert et al., 2013; Zemke et al., 2009).

Wnt Signaling Is Required in a Stage-Dependent Manner for Normal Lung Epithelial Specification

Having identified Wnt signaling as a putative patterning pathway, we sought to understand more about the stage-dependent role of this pathway in hPSC lung differentiation. By comparing iPSC-derived anterior foregut endoderm to purified NKX2-1^{GFP+} progenitors at day 15 of differentiation through unbiased gene set enrichment analysis (GSEA) of their global transcriptomes, we identified 19/50 gene sets statistically upregulated in day 15 NKX2-1^{+} progenitors (false discovery rate [FDR] <0.1), including Wnt/β-catenin signaling (Table S1). Upregulation of the canonical target Wnt genes, *AXIN2*, *NKD1*, and *LEF1* and downregulation of the Wnt inhibitor *DKK1* were particularly predictive of Wnt activity in this system (Figure 2A). These changes were maintained until day 28 in NKX2-1^{+} cells cultured in media containing CHIR (Figure S2A). The faithfulness of *AXIN2* as a canonical Wnt response reporter in this human system was further supported by separate experiments where lentiviral overexpression of phosphorylation-incompetent murine β-catenin (Fuerer and Nusse, 2010) in NKX2-1^{+} progenitors resulted in upregulation of *AXIN2* even in the absence of CHIR (Figures S2B and S2C). Furthermore, lentiviral TCF reporters in FG293 cells confirmed that the dose of CHIR used at this stage and later differentiation (3 μM) was appropriate to induce Wnt activation without significant cytotoxicity (Figures S2D and S2E).

Next, we compared the stage-dependent effects of withdrawal of Wnt signaling pre- versus post-lung specification in our directed differentiation model using both CHIR and recombinant Wnt3a (Figure S3A). Cells differentiated from anterior foregut endoderm in the presence of CHIR expressed significantly higher levels of NKX2-1^{GFP} as early as 48 hr after the initiation of specification in comparison to cells cultured without this compound, and this difference was maintained until at least day 15.

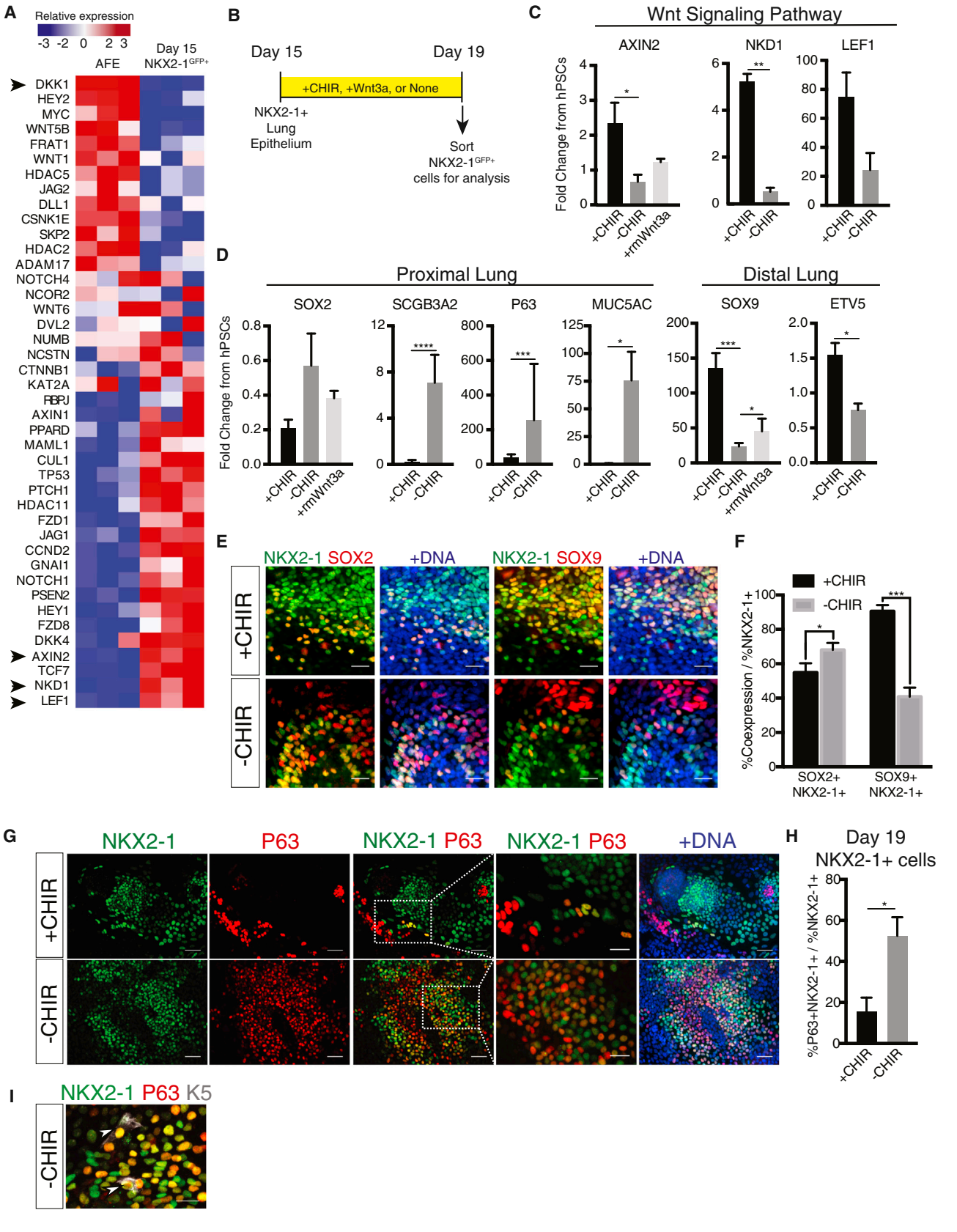

(legend on next page)

NKX2-1^{GFP} expression could not be rescued in cells differentiated without CHIR to day 15 by later CHIR addition, suggesting that this effect was restricted to a narrow developmental stage (Figure S3B). Activation of canonical Wnt signaling in response to CHIR at these time points was verified using lentiviral TCF-driven reporters, and conditions without CHIR again exhibited minimal, if any, basal Wnt activity (Figures S3C and S3D). Together, these results support the conclusion that canonical Wnt activity is required for in vitro specification of human lung epithelial progenitors in a narrow window of developmental competence.

CHIR Withdrawal Post Lung Epithelial Specification Results in Loss of Distal Lung Patterning and the Emergence of Proximal Lung Lineages, Including NKX2-1^{+}TP63^{+} Basal-like Cells

Next, we tested the effect of sustained versus withdrawn Wnt signaling on the differentiation repertoire of hPSC-derived NKX2-1^{+} progenitors after lung lineage specification. We treated cells post-specification with CHIR, recombinant mouse Wnt3a, or neither in a base media of 10 ng/mL FGF10 from day 15 to day 19 (Figures 2B and S3E). To ensure this treatment correlated with expected decreases in canonical Wnt signaling activity, we confirmed reduced lentiviral TCF-driven reporter expression by day 19 (Figure S3F) as well as reduced expression of the Wnt signaling responsive genes *LEF1*, *NKD1*, and *AXIN2* (Figure 2C). An unbiased comparison between NKX2-1^{GFP+} cells at day 15 and at day 19 after culture without CHIR using a Wnt pathway-specific qRT-PCR array further confirmed this finding (Figure S3G).

Within 4 days, withdrawal of CHIR resulted in significant changes in gene expression suggesting emergence of a proximal airway phenotype concordant with loss of distal cell fate in NKX2-1^{GFP+} cells. Specifically, proximal airway markers *SCGB3A2*, *TP63*, and *MUC5AC* were upregulated and distal markers *SOX9* and *ETV5* (Liu et al., 2003) were downregulated in response to CHIR withdrawal (Figure 2D). Patterning of individual NKX2-1^{+} cells in response to CHIR withdrawal was validated at the protein level by both immunofluorescence microscopy and flow cytometry. Triple immunostaining for NKX2-1, SOX2, and SOX9 nuclear proteins demonstrated that >90% of NKX2-1^{+} cells were SOX9^{+} in the presence of sustained CHIR, whereas 4 days after the withdrawal of CHIR, <40% of NKX2-1^{+} cells maintained detectable SOX9 staining (Figures 2E and 2F). Although NKX2-1^{+} cells in both conditions contained >50% SOX2^{+} cells, CHIR withdrawal resulted in a significantly higher percentage of cells coexpressing NKX2-1 and SOX2 and a concordant absence of SOX9 in the majority of these NKX2-1^{+}/SOX2^{+} cells (Figures 2E, 2F, and S4A). This result further revealed a number of cells in both outgrowth conditions simultaneously expressing NKX2-1, SOX2, and SOX9 (Figure S4B), a triad that has not been observed to date in murine models of development and may represent a phenomenon unique to the human lung.

Furthermore, CHIR withdrawal resulted in increased frequencies of cells co-expressing NKX2-1 and TP63 (Figures 2G and 2H) and a subset of cells co-expressing NKX2-1, TP63, and K5, a triad unique to airway basal cells (Figure 2I) (Ikeda et al., 1995; Rock et al., 2009). Cells treated with rhWnt3a during this same window showed a milder distal patterning response relative to CHIR treatment (Figures 2C and 2D) with only partial activation of canonical Wnt activity detected as measured by *AXIN2* expression, concordant with the previously reported low-level response of human cells to recombinant Wnt (Fuerer and Nusse, 2010).

CHIR Acts Intrinsically on the Epithelium to Pattern Early Lung Progenitors

Withdrawal of CHIR from day 15 to day 19 resulted in a significantly decreased percentage of NKX2-1^{GFP+} outgrowth by day 19 (Figures S4C and S4D), raising the question of whether non-lung lineages were outcompeting lung lineages and potentially contributing to secondary patterning effects in the NKX2-1^{+} population in the absence of sustained Wnt. We therefore sought to

Figure 2. Withdrawal of Wnt Signaling Activity Post-lung Specification Leads to Increased Proximal Patterning

(A) Gene set enrichment analysis (GSEA) of microarray data indicating the unbiased ranking of Wnt pathway genes differentially expressed comparing iPSC-derived day 6 ("anterior foregut endoderm," or "AFE") cells and day 15 purified NKX2.1^{GFP+} cells. Arrowheads, Wnt target genes anticipated to be most predictive of signaling activity.

(B) Schematic of experiment showing manipulation of Wnt signaling from days 15–19.

(C) qRT-PCR showing fold change in gene expression compared to day 0 ($2^{-\Delta\Delta Ct}$) in day 19 NKX2-1^{GFP}-sorted cells after 4 days treatment ± CHIR or rmWnt3a. Bars represent mean ± SEM. +CHIR, n = 9 biological replicates of independent wells within multiple differentiations; +rmWnt3a, n = 3. *p ≤ 0.05, **p ≤ 0.01, ***p ≤ 0.001, ****p ≤ 0.0001 by unpaired, two-tailed Student's t test.

(D) Fold change of mRNA expression in NKX2-1^{GFP+} cells on day 19 over undifferentiated iPSCs. Unsorted cells were cultured with or without CHIR or rmWnt3a (SOX2, SOX9) from days 15–19 then GFP^{+} cells were sorted on day 19. Bars represent mean ± SEM. Biological replicates for each condition: CHIR treatment SOX2, n = 9; SCGB3A2, TP63, n = 10; SOX9, n = 6; MUC5AC, ETV5, n = 3. For rmWnt3a, n = 3. *p ≤ 0.05, **p ≤ 0.01, ***p ≤ 0.001, ****p ≤ 0.0001 by unpaired, two-tailed Student's t test.

(E) Representative immunofluorescence stains of NKX2-1 (green) and SOX2 or SOX9 (red) protein expression with DNA stain (Hoechst; blue) at day 19 with and without CHIR from days 15–19. Panels are images of the same cells stained for all three markers. Scale bars, 25 μm.

(F) Quantification of NKX2-1, SOX2, and SOX9 coexpression by intracellular flow cytometry (SOX2) or by colocalization calculated from staining in (E) (SOX9). Bars represent mean ± SD, n = 3 biological replicates. *p = 0.03; ***p = 0.0002 by unpaired two-tailed Student's t test.

(G) Representative immunofluorescence stains for NKX2-1 (green) and TP63 (red) nuclear protein expression with DNA stain (Hoechst; blue) at day 19 with and without CHIR from days 15–19. Left panels and right panel: scale bars, 50 μm. Second from right panel: scale bars, 25 μm.

(H) Quantification of NKX2-1 and TP63 colocalization from staining in (G). Bars represent mean ± SD, area from five images each of n = 3 biological replicates. *p = 0.01 by unpaired two-tailed Student's t test.

(I) Immunofluorescence of NKX2-1 (green), TP63 (red), and KRT5 (white) at day 19 after culture without CHIR from days 15–19. Arrowheads, triple positive cells. Scale bars, 50 μm.

See also Figures S2–S4.

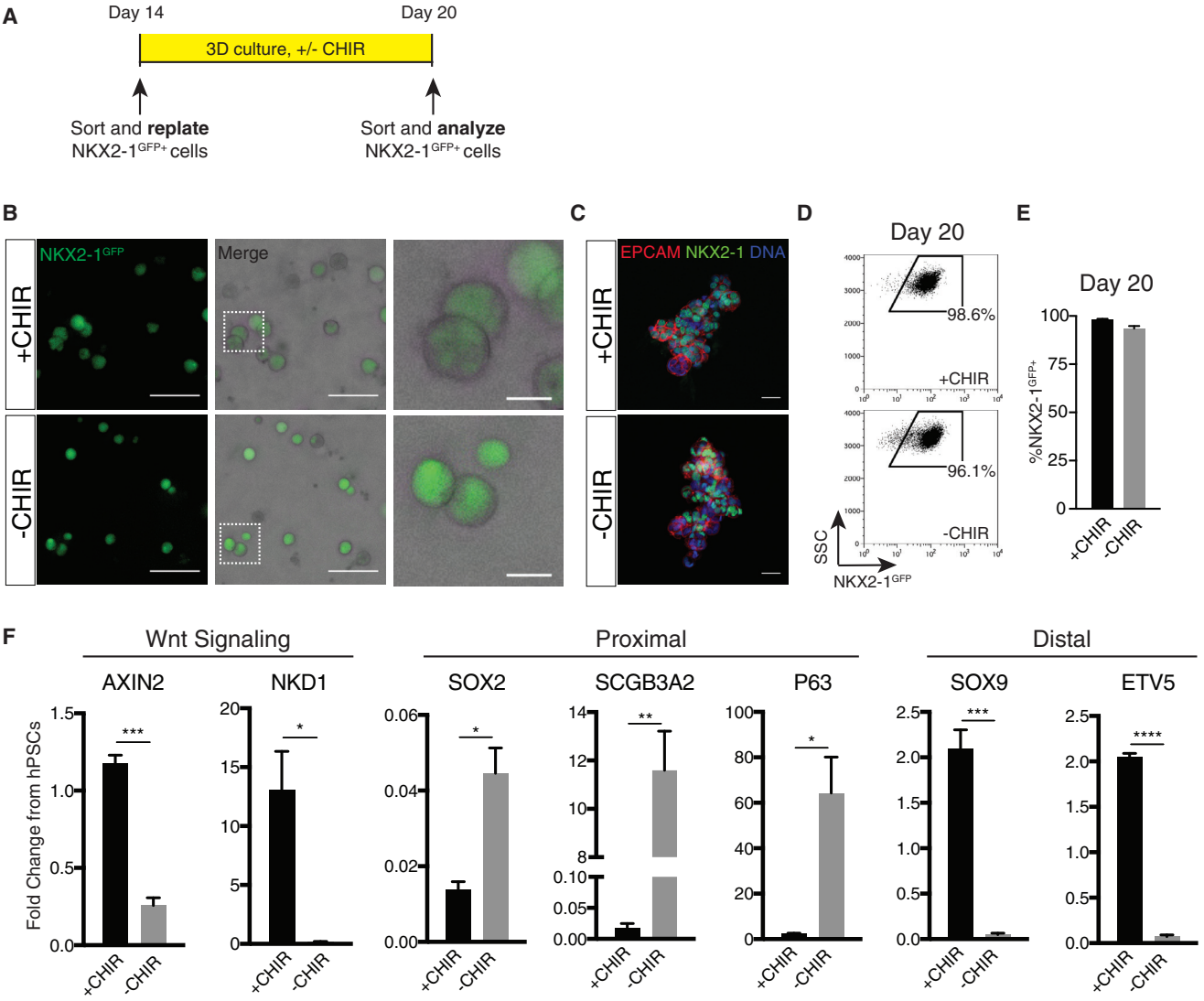

Figure 3. Inhibition of Proximal Patterning by Wnt Activation Is Intrinsic to the NKX2-1^{+} Lung Epithelium

(A) Experimental design for testing CHIR effects on purified NKX2-1^{GFP+} endodermal lung progenitors.

(B) Live cell fluorescence microscopy on day 20, depicting NKX2-1^{GFP} in iPSC-derived organoids treated with and without CHIR from days 14–20 (6 days post-sort). Scale bars, 100 μm (left and center panels); 25 μm (right panel). Dashed boxes represent zoom views.

(C) Whole-mount immunofluorescence images of EPCAM (red) and NKX2-1 (green) expression in day 20 organoids. Scale bars, 25 μm.

(D) NKX2-1^{GFP} flow cytometry analysis of organoids on day 20.

(E) Quantification of analysis from (D). Bars represent mean ± SD, n = 3.

(F) Fold change of genes in NKX2-1^{GFP+} cells on day 20 over undifferentiated iPSCs by qRT-PCR ($2^{-\Delta\Delta Ct}$). Bars represent mean ± SD, n = 3 biological replicates from independently sorted wells of a differentiation. *p ≤ 0.05, **p ≤ 0.01, ***p ≤ 0.001, ****p ≤ 0.0001 by unpaired, two-tailed Student's t test.

test whether the effect of CHIR manipulation on proximodistal lung patterning was intrinsic to lung epithelial cells. We used fluorescence-activated cell sorting (FACS) to purify NKX2-1^{GFP+} epithelial lung progenitors at day 14 and replated them in three-dimensional (3D) culture with or without CHIR (Figure 3A) added to a base media ("DCI") that we have previously shown supports epithelial gene expression in sorted NKX2-1^{GFP+} PSC-derived cells (Hawkins et al., 2017; Kurmann et al., 2015; Longmire et al., 2012). By day 20, the sorted cells formed small spheres coexpressing NKX2-1 and EPCAM (Figures 3B and 3C). Greater than 90% of all outgrowth cells in either culture condition maintained NKX2-1^{GFP} expression (+CHIR: 98.2% ± 0.5%; −CHIR: 93.4% ± 2.3%) (Figures 3D and 3E), and cells in each condition formed organoids with no measured statistical difference in efficiency. Analysis of re-sorted NKX2-1^{GFP+} cells at day 20 demonstrated withdrawal of CHIR resulted in downregulation of Wnt pathway markers and concurrent upregulation of proximal lung genes *SOX2*, *SCGB3A2*, and *TP63*, and downregulation of distal lung genes *SOX9* and *ETV5* (Figure 3F). These results suggested that Wnt signaling levels regulate proximodistal patterning of NKX2-1+ lung progenitors via intrinsic actions on the epithelium.

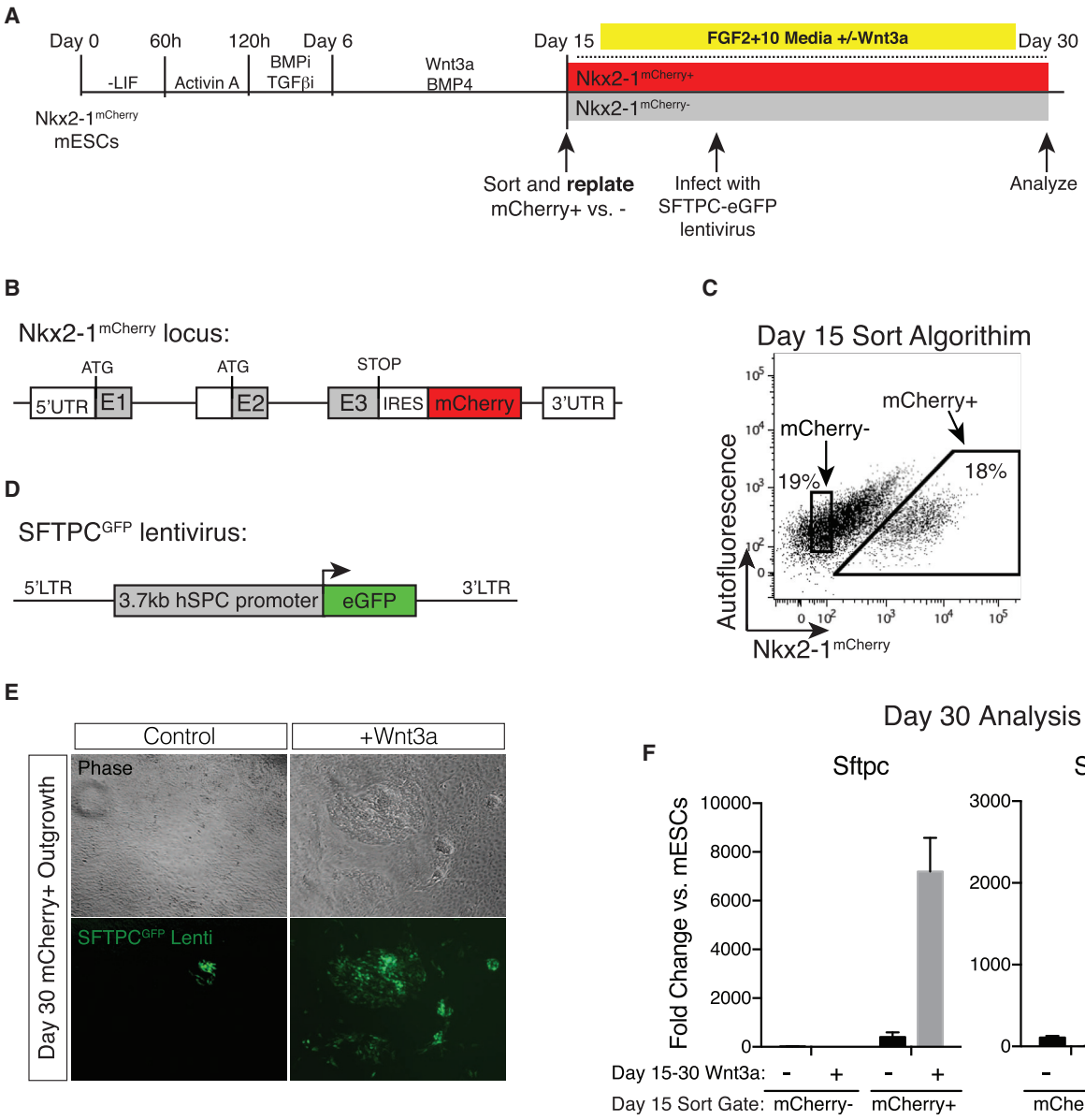

Figure 4. Mouse Embryonic Stem Cell-Derived Nkx2-1$^{mCherry+}$ Lung Progenitors Upregulate Sftpc in Response to Wnt3a

(A) Schematic depicting directed differentiation of Nkx2-1$^{mCherry+}$ cells from mouse embryonic stem cells (mESCs) and transduction of sorted cells with Sftpc^{GFP} reporter lentivirus.

(B) Schematic of targeted Nkx2-1^{mCherry} locus.

(C) Representative flow cytometry plot with gates for day 15 mCherry^{+} versus mCherry^{-} sort.

(D) Schematic of Sftpc^{GFP} lentivirus.

(E) Representative images showing induction of the Sftpc^{GFP} reporter in cells from the Nkx2-1$^{mCherry+}$ outgrowth treated with rmWnt3a.

(F) Fold change of mRNA expression for Sftpc and Scgb1a1 in outgrowth of Nkx2-1$^{mCherry+}$ versus Nkx2-1$^{mCherry-}$ cells sorted on day 15 and analyzed on day 30 by qRT-PCR ($2^{-\Delta\Delta Ct}$; fold change compared to day 0 mESCs). Bars represent mean ± SD, n = 2 biological replicates.

Recombinant Wnt3a Promotes Sftpc Expression and Inhibits Proximalization in Nkx2-1^{+} Mouse ESC-Derived Lung Progenitors

Next, we sought to test whether the patterning response to canonical Wnt signaling is conserved in other mammalian PSC model systems known to respond directly to Wnt ligands. As we have previously described the use of Wnt3a to drive lung differentiation in murine PSCs (Kurmann et al., 2015; Longmire et al., 2012) (Figure 4A) and because genetic mouse models demonstrate a role for canonical Wnt signaling in proximodistal patterning (Hashimoto et al., 2012; Mucenski et al., 2003; Shu et al., 2005), we differentiated a mouse embryonic stem cell (mESC) line containing an mCherry reporter targeted to the Nkx2-1 locus (Bilodeau et al., 2014; Kurmann et al., 2015) (Figure 4B). Following lung lineage specification into Nkx2-1^{+} primordial progenitors, on day 14 we replated sorted

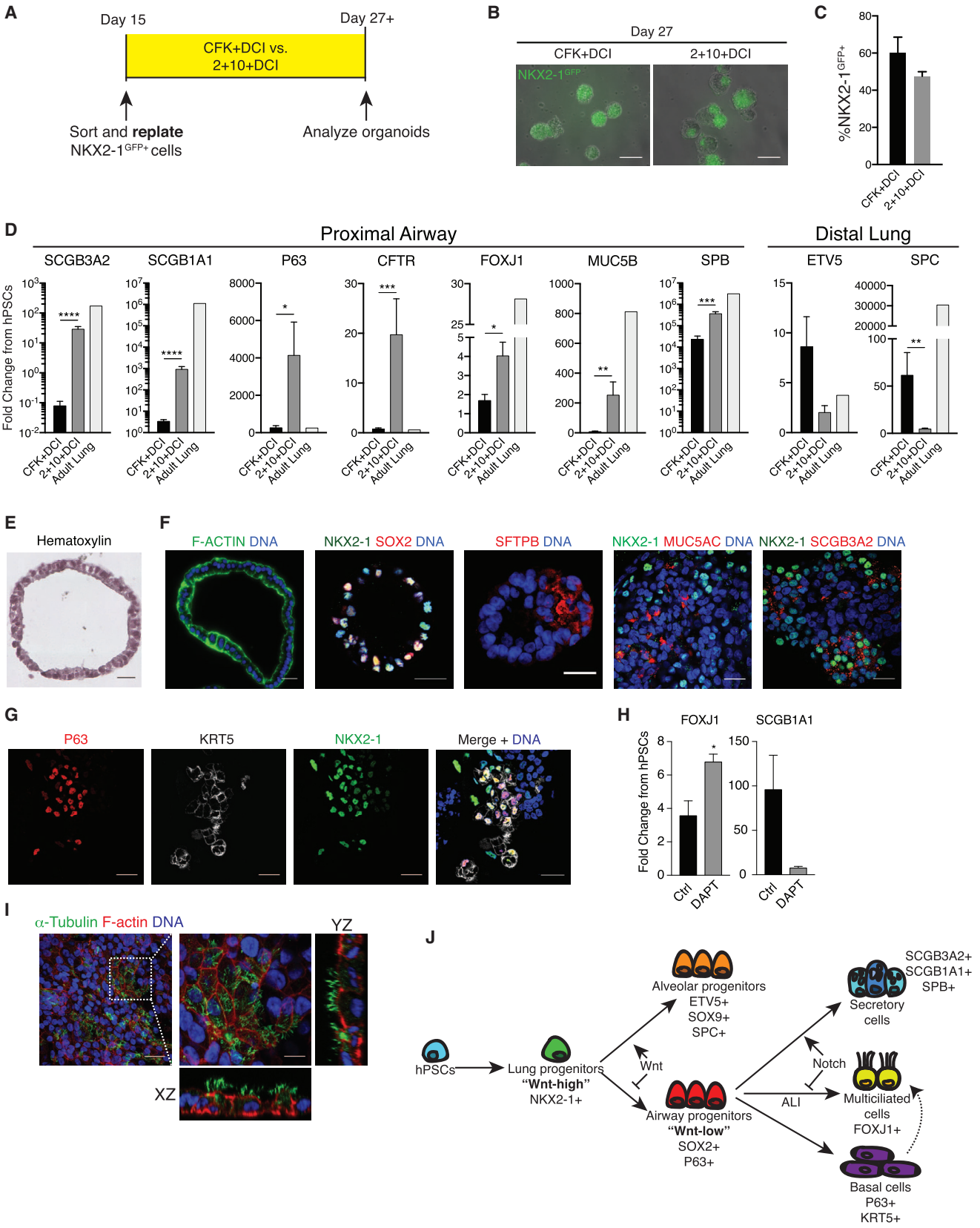

(legend on next page)

Nkx2-1$^{mCherry+}$ versus Nkx2-1$^{mCherry-}$ cells (Figure 4C) for further differentiation in sustained versus withdrawn Wnt3a protein. By transducing these cells with a reporter lentivirus carrying a human *SFTPC* promoter driving GFP expression (Longmire et al., 2012), we then screened for the emergence of lung cells expressing this canonical distal epithelial differentiation marker (Figure 4D). By day 18, we observed the emergence of many clusters of Sftpc^{GFP+} cells deriving from mCherry^{+}-sorted progenitors cultured in the presence of Wnt3a, but few, if any, detectable clusters in the absence of Wnt3a (Figure 4E). As accurately predicted by the Sftpc^{GFP} reporter, *Sftpc* mRNA was expressed at high levels in the presence of Wnt3a and proximal lung marker *Scgb1a1* expression was suppressed in these conditions. In contrast, in the absence of Wnt3a, *Scgb1a1* expression was upregulated and *Sftpc* expression was almost entirely lost (Figure 4F), findings consistent with our human PSC model. Importantly, no detectable GFP signal and no *Sftpc* or *Scgb1a1* mRNA expression was observed arising from outgrowth of the sorted mCherry negative population in any condition (Figure 4F). These results provide further evidence that canonical Wnt activation promotes the differentiation of distal lung epithelium from PSC-derived Nkx2-1^{+} lung progenitors while suppressing the proximal lung program and this effect is conserved across species.

Derivation of Proximal Airway Organoids from Purified PSC-Derived Lung Epithelial Cells

Having demonstrated that Wnt manipulation acts intrinsically on NKX2-1^{+} lung epithelium to induce rapid changes in proximodistal patterning, we sought to develop a "low-Wnt" protocol for the reproducible and efficient generation and maturation of functional proximal airway organoids from patient-specific lines for the purposes of disease modeling and the testing of gene therapies. Our results from 2D mESC differentiations (Figure 4) indicated that media containing FGF2 and FGF10 ("2+10 media") to broadly ligate FGF receptors would drive proliferation of sorted NKX2-1^{GFP+} lung progenitors while allowing proximal patterning, results in keeping with our previously published use of 2+10 media (Longmire et al., 2012). We therefore tested whether in 3D conditions 2+10 media without CHIR or Wnt3a would result in proliferation and differentiation of proximalized human lung epithelial spheres in comparison to previously published high-Wnt media containing CHIR as well as FGF10 and KGF ("CFK media") (Hawkins et al., 2017; Huang et al., 2014) (Figure 5A).

To ensure that organoids originated from an NKX2-1^{+} progenitor population, sorted NKX2-1^{GFP+} cells were replated and cultured in both "high Wnt" and "low Wnt" conditions in 3D. Cells in both conditions initially proliferated and formed epithelial spheres that maintained variable levels of NKX2-1 expression (Figures 5B and 5C). However, the spheres that formed in low-Wnt media expressed significantly higher levels of proximal airway genes than cells in high-Wnt media, including *TP63*, *SCGB3A2*, *SCGB1A1*, *MUC5B*, *CFTR*, *FOXJ1*, and *SFTPB* (Figure 5D). Although *SFTPB* has previously been referred to as a marker specific to type II pneumocytes, it is also highly expressed in the developing human airway epithelium (Phelps and Floros, 1988). In contrast, cells cultured in high-Wnt media again expressed lower levels of proximal lung markers and higher levels of distal lung markers *ETV5* and *SFTPC* (Figure 5D). Expression of additional distal alveolar epithelial markers, *ABCA3* and *LPCAT1*, was also detected in cells cultured in high-Wnt media (data not shown).

Airway-like epithelial identity of the low-Wnt outgrowth was supported by immunostaining revealing luminal organoids where all cells expressed EPCAM and SOX2 and subsets expressed markers of secretory (SPB^{+}/NKX2-1^{+}; SCGB3A2^{+}/NKX2-1^{+}), goblet (MUC5AC^{+}NKX2-1^{-}), and basal (NKX2-1^{+}/TP63^{+}/KRT5^{+}) lung lineages (Figures 5F, 5G, and S5A–S5F). These spheres were initially primarily secretory and basal in nature and exhibited low levels of *FOXJ1* expression with no observed formation of multiciliated structures. However, multiciliated epithelial cells with upregulated *FOXJ1*, downregulated *SCGB1A1*, and beating motile cilia could be generated from these proximalized epithelial spheres within 2 weeks either in continued 3D culture in the presence of Notch inhibition with DAPT (Tsao et al., 2009) (Figure 5H; Movie S1) or after transfer into 2D conditions in air liquid interface culture (Figures 5I and S5G).

Taken together, these results suggested the proximalized airway spheres generated in low-Wnt conditions resemble airway epithelium and provide a mechanistic roadmap by which hPSC-derived NKX2-1^{+} lung progenitors can be differentiated to

Figure 5. Generation of iPSC-Derived Airway Organoids via Purified NKX2-1^{+} Lung Progenitors

(A) Schematic depicting protocol for differentiating organoids from purified NKX2-1^{GFP+} progenitors.

(B) Representative fluorescence microscopy for NKX2-1^{GFP} expression in organoids cultured in distalizing (Wnt-high; CFK+DCI versus proximalizing (Wnt-low; 2+10+DCI) conditions until day 27. Scale bars, 50 μm.

(C) Quantification of NKX2-1^{GFP} expression in CFK+DCI and 2+10+DCI organoids at day 27 by flow cytometry. Bars represent mean ± SEM, n = 6 biological replicates from independent wells of multiple differentiations.

(D) Fold change of mRNA expression in day 27 organoids and adult lung control over undifferentiated iPSCs by qRT-PCR ($2^{-\Delta\Delta Ct}$). Bars represent mean ± SEM, n = 6 biological replicates from independent wells of multiple differentiations. *p ≤ 0.05, **p ≤ 0.01, ***p ≤ 0.001, ****p ≤ 0.0001 by unpaired, two-tailed Student's t test.

(E) Hematoxylin staining of sectioned organoid.

(F) Representative whole mount immunofluorescence staining for indicated markers. Scale bars, 25 μm.

(G) Representative whole mount immunofluorescence staining for lung basal cell markers. Scale bars, 25 μm.

(H) Fold change of mRNA expression in 2+10+DCI organoids cultured with DAPT or vehicle alone for 2 weeks (days 31–45). Bars represent mean ± SD, n = 3 biological replicates from one differentiation, *p ≤ 0.05 by unpaired, two-tailed Student's t test.

(I) Representative z projection and orthogonal projections of acetylated alpha-tubulin and f-actin staining of 9-day air-liquid interface culture generated from replated outgrowth of proximalized organoids. Scale bar, 25 μm (upper panel); 10 μm (lower panel).

(J) Schematic depicting proposed pathways for the generation of proximal or distal lung lineages.

See also Figure S5 and Movie S1.

diverse lineages of distinct clinical interest (Figure 5J). In particular, identification of Wnt signaling as a key regulator of proximodistal patterning is a critical step for the rapid and reproducible generation from hPSC lines of proximal lung epithelial NKX2-1^{+}/SOX2^{+} progenitors and their downstream basal, secretory, or multiciliated progeny.

CFTR-Dependent Forskolin Swelling of Proximalized Organoids

To test whether the organoids differentiated in our proximalized lung protocol contained functional epithelia of potential clinical benefit for cystic fibrosis disease modeling, we next sought to develop an in vitro quantitative assessment of epithelial CFTR function using patient-specific iPSC-derived airway organoids. It has been previously reported in non-lung systems that the activation of adenylyl cyclase by forskolin induces CFTR-dependent organoid swelling, providing a robust and quantifiable in vitro functional readout of this ion channel (Dekkers et al., 2013). To initially test whether our airway organoids swell in response to forskolin treatment, we differentiated iPSCs derived from either a healthy individual (BU3) or two individuals with cystic fibrosis due to homozygous ΔF508 CFTR mutations (RC2 202 and RC2 204). To purify NKX2-1^{+} primordial lung progenitors without requiring NKX2-1^{GFP} knockin reporters, we used the cell surface markers CD47 and CD26 to isolate CD47^{hi}CD26^{-} cells that are highly enriched in NKX2-1^{+} progenitors by day 15 from all three lines (Hawkins et al., 2017) (Figure S6A). Importantly, sorted progenitors from all lines replated from day 15 to days 22–35 showed a similar proximalized patterning response to withdrawal of CHIR and expansion in 2+10 media as our C17 NKX2-1^{GFP}-targeted line (Figure S6B and data not shown), suggesting that this protocol reproducibly generates airway organoids from lung progenitors derived from different hPSC lines purified using cell surface marker sorting.

By time-lapse microscopy of BU3-derived organoids after exposure to forskolin, we detected swelling beginning within 60 min, resulting in quantifiable changes in surface area evident within 3 hr and continuing for at least 20 hr (2.07- ± 0.6-fold at t = 20 hr, Figures S6C and S6D). In contrast, little, if any, swelling was observed in either cystic fibrosis line (RC2 202 or RC2 204) after exposure to forskolin or in BU3 organoids stimulated with carrier vehicle alone (PBS only: 1.02 ± 0.03, Figures S6C and S6D). Having observed forskolin-responsive swelling in normal and not cystic fibrosis patient-derived proximalized organoids, we sought to establish whether this response was CFTR-dependent. To test this, we used gene edited clones we have previously generated from both cystic fibrosis lines (Crane et al., 2015) where one ΔF508 mutant allele has been corrected to wild-type sequence (Crane et al., 2015). To compare the two diseased (ΔF508/ΔF508) iPSC lines to their syngeneic heterozygous corrected progeny (ΔF508/wild-type [WT]), we differentiated all four clones to the lung progenitor stage (Figure 6A) and purified each differentiated line using our CD47^{hi}/CD26^{-} sort algorithm (Figure 6B) and differentiated the organoids further in our "low-Wnt" media (Figure 6C). After proximalization, the gene corrected ΔF508/WT RC2 202 and 204 organoids significantly swelled in response to forskolin treatment (1.73- ± 0.15-fold and 1.32- ± 0.09-fold, respectively; average rate of swelling for RC2 202 = 0.067-fold/hr ± 0.059 in the first 2.5 hr and 0.025-fold/hr ± 0.013 in the subsequent 22 hr; Figures 6D–6F). These values were comparable to swelling observed in the normal (BU3) organoids (Figure S6D). In contrast, the ΔF508/ΔF508 homozygous parental lines again showed no significant swelling in the same conditions (Figures 6D–6F and S6E; Movies S2 and S3) Taken together, these results support the conclusion that proximalized iPSC-derived lung organoids contain functional epithelial cells with the potential for in vitro lung-specific disease modeling and gene correction of cystic fibrosis.

DISCUSSION

Our results demonstrate the directed differentiation of PSCs into functional airway epithelial cells via an NKX2-1^{+} progenitor intermediate in response to cyclical modulation of developmental signaling pathways. Using genetic mouse models to inform pathway screening during a narrow 4-day window post-lung specification, we identified Wnt signaling as a potent and key regulator of proximodistal patterning in both human and mouse PSC-derived lung epithelium. Our in vitro findings significantly extend prior observations made in mice in vivo, and suggest that developing human airway epithelia are similarly patterned by oscillations in levels of canonical Wnt signaling. For example, prior published mouse studies emphasize a requirement for Wnt signaling during the narrow developmental window of lung specification (Goss et al., 2009; Harris-Johnson et al., 2009) followed by alterations in Wnt signaling levels to regulate proximodistal patterning. In particular, it has been demonstrated that Wnt inhibition in mice promotes increases in proximalization at the expense of distal lineages (Mucenski et al., 2003; Shu et al., 2005; Volckaert et al., 2013). In contrast, forced activation of Wnt signaling maintains distal lung progenitor programs while suppressing proximalization (Hashimoto et al., 2012; Li et al., 2009). In some models, forced hyperactivation of canonical Wnt signaling during mouse lung development blocks club cell differentiation (Hashimoto et al., 2012) or activates aberrant gastrointestinal gene expression programs in the lung epithelium (Okubo and Hogan, 2004). Interestingly, Wnt activation or inactivation in post-natal proximalized mouse lung epithelia does not result in loss of patterning (Reynolds et al., 2008; Zemke et al., 2009) in the absence of injury but has been correlated with airway epithelial dysregulation in adult human smokers (Wang et al., 2011).

Similarly, we find that although Wnt signaling is essential for specification of respiratory progenitors from hPSCs, withdrawal of Wnt post-specification promotes rapid emergence of the proximal airway program and abrogation of distal lung fate via a mechanism intrinsic to the NKX2-1^{+} epithelium. This latter finding is critical, as previous genetic mouse models have emphasized both patterning and epithelial branching morphogenesis defects in the context of abnormal Wnt signaling. In contrast, our model provides interrogation of epithelial-specific effects of Wnt signaling distinct from defects in lung structure or branching.

In contrast to previously described iPSC protocols using extended culture conditions to generate cell types of interest (Gotoh et al., 2014; Konishi et al., 2016), the rapidity and stage-specificity of Wnt-driven proximodistal airway patterning strongly supports our interpretation that temporal oscillations

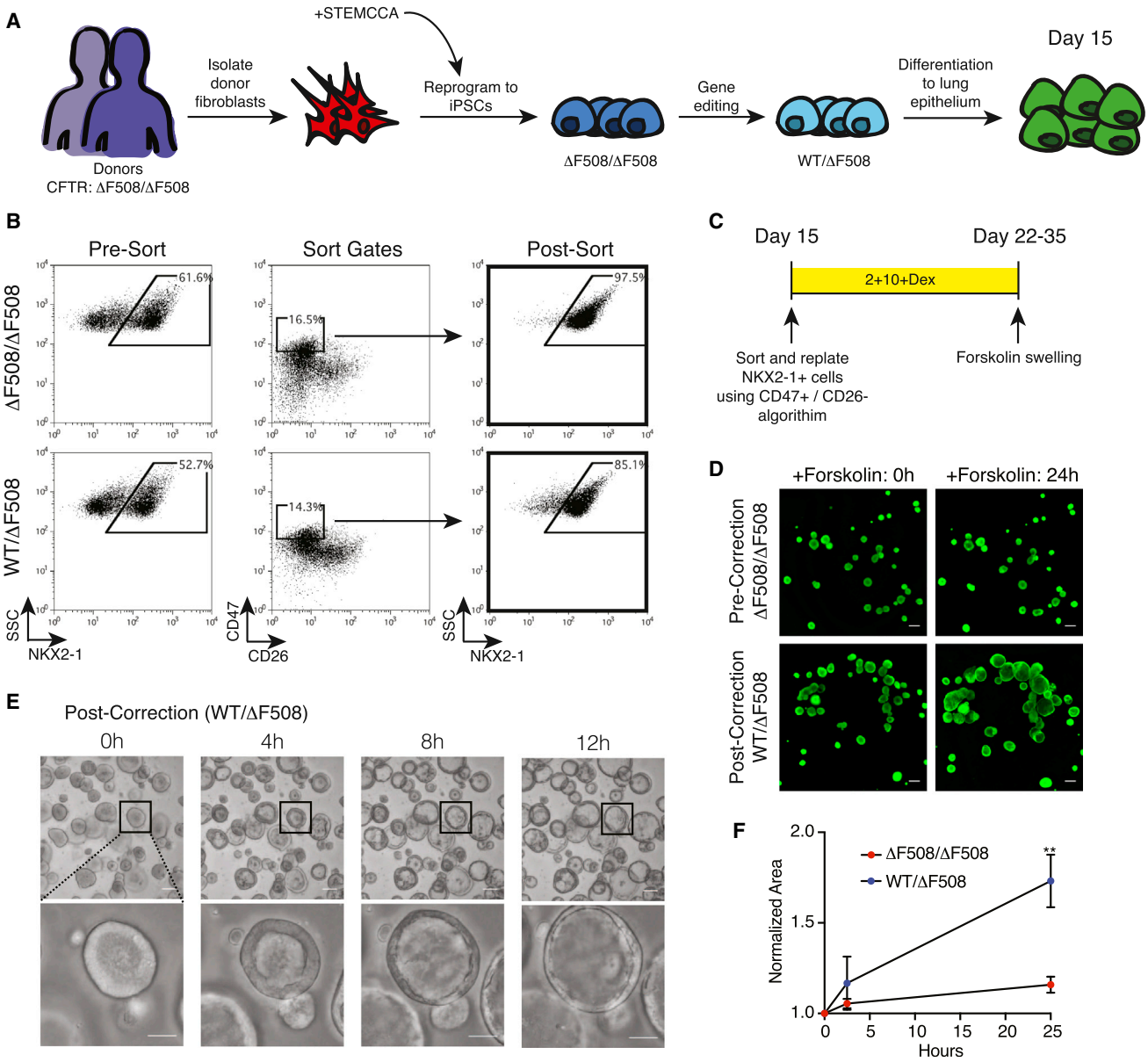

Figure 6. Functional Assessment of Gene Edited, Cystic Fibrosis Patient-Specific iPSC-Derived Airway Organoids Indicates a CFTR-Dependent Forskolin Swelling Response

(A) Schematics depicting the generation, gene correction, and differentiation of syngeneic ΔF508/ΔF508 and ΔF508/WT cystic fibrosis patient-derived hPSC lines.

(B) Representative flow cytometry analysis of intracellular NKX2-1 expression pre- and post-CD47^{hi}/CD26^{-} sorting of uncorrected and corrected cystic fibrosis iPSC line RC2 204. Middle plots show typical CD47/CD26 sort gating strategy.

(C) Schematic describing post-sort outgrowth of differentiated cells.

(D) Fluorescence microscopy of live (calcein green stained) organoids from pre- and post-corrected iPSC line RC2 202 at time = 0 hr and time = 24 hr post-forskolin treatment. Scale bars, 100 μm.

(E) Time-lapse phase contrast microscopy of forskolin-treated, gene-corrected (ΔF508/WT) organoids from RC2 204.

(F) Quantification of normalized swelling area of organoids derived from pre- and post-corrected clones of RC2 202 at time = 0, 3, and 25 hr. Calcein green stained area for each well set to 1 at time = 0 hr. Bars represent mean ± SD, n = 3 biological replicates from independent wells of a differentiation. p = 0.0038 by unpaired, two-tailed Student's t test.

See also Figure S6 and Movies S2 and S3.

in signaling pathway activation are a critical component of effective directed airway differentiation. Building on these findings, we generated the novel "low-Wnt" protocol presented here for the derivation of airway organoids from purified NKX2-1^{+} lung epithelial progenitors. Although we demonstrate that FGF signaling does not block the initial proximal patterning of these

cells, we have not ruled out the possibility that this pathway, stimulated by FGFs added as trophic factors to our base media, might contribute to the subsequent differentiation of proximal cell types within these organoids.

In our characterization and optimization of this "low-Wnt" protocol, three key features of our approach are unique. First, the use of an NKX2-1^{GFP} knockin reporter has allowed us to dissect lineage relationships, establishing that our proximal airway epithelia derive directly from an NKX2-1^{+} lung progenitor intermediate. Second, the ability to modulate Wnt signaling in these purified NKX2-1^{+} "epithelial only" derivatives allows testing of intrinsic pathway effects separated from the potentially confounding responses of mesenchymal or other NKX2-1^{-} lineages that are frequently present in unsorted heterogeneous PSC experiments. Third, the rapid, patterned response of our sorted lung progenitors to withdrawal of Wnt (augmented proximalization concordant with loss of distalization within 4 days) suggests that directed developmental patterning is occurring rather than the overgrowth of competing proximal lineages that can occur with prolonged culture periods. While we cannot completely exclude the possibility that selection of lineage restricted cells, rather than the patterning of bipotent or equipotent NKX2-1^{+} day 15 progenitors is occurring in our protocol, the rapidity of the large-scale changes in SOX9 versus SOX2 expression patterns in response to Wnt withdrawal argues against this possibility.

The end result of our approach is the production of a potentially inexhaustible source of human proximal airway organoids. These luminal structures contain multiple airway epithelial lineages and express airway markers at levels comparable to the adult lung. As predicted by murine models, inhibition of Notch signaling in these organoids or subsequent 2D air-liquid interface culture results in ciliogenesis in a subset of cells (You et al., 2002; Firth et al., 2014; Konishi et al., 2016) and provides evidence for our conclusion that organoids grown from purified NKX2-1^{+} lung epithelial cells in the absence of CHIR represent proximalized airway progenitors that respond as predicted to developmental signaling cues.

One important goal of our work is the engineering of clinically applicable patient-specific in vitro models of airway epithelial disease and epithelial function. Thus, we have developed cell-sorting algorithms (CD47^{hi}/CD26^{-}) that enable the isolation of iPSC-derived NKX2-1^{+} lung progenitors possessing airway organoid competence without the need to generate NKX2-1^{GFP} knockin reporters for each patient-specific line to be studied. We employ this sorting algorithm and our proximalization approach to produce patient-specific airway epithelial organoids both before and after gene editing to correct the CFTR genetic lesion responsible for cystic fibrosis. These airway organoids allow in vitro forskolin stimulation assays to analyze CFTR function in lung epithelial cells. A logical priority in future studies will be testing whether our patient-specific airway organoid model of cystic fibrosis more closely recapitulates the airway disease phenotypes or known person-to-person variability in disease manifestations compared to previously published and more invasive models of CFTR function that are based on non-lung cells, such as primary intestinal cell-derived forskolin-induced swelling assays (Dekkers et al., 2013). Beyond cystic fibrosis, the iPSC airway organoid system may also be readily adaptable for in vitro modeling and drug development for other inherited diseases of the airway, such as primary ciliary dyskinesia.

In summary, the findings presented here demonstrate the rapid generation of airway organoids by stage-dependent modulation of Wnt signaling and proof-of-principle for the utility of these organoids in lung disease modeling. Thus, we have developed a human in vitro PSC-based model system able to reveal basic mechanisms regulating lung developmental cell fate decisions and model airway epithelial diseases with potential clinical benefit for precision drug screening and regenerative medicine.

STAR★METHODS

Detailed methods are provided in the online version of this paper and include the following:

- KEY RESOURCES TABLE
- CONTACT FOR REAGENT AND RESOURCE SHARING
- EXPERIMENTAL MODEL AND SUBJECT DETAILS
  - Human ESC/iPSC Reporter Line Generation and Maintenance
  - Mouse ESC Reporter Line Maintenance
- METHOD DETAILS
  - Directed Differentiation of hPSCs
  - Purification of NKX2-1+ Lung Progenitors by Cell Sorting
  - Post-Specification Patterning of Lung Epithelial Progenitors
  - Gene Set Enrichment Analysis
  - Generation of Lentiviral Reporters for Wnt Signaling
  - Reverse Transcriptase Quantitative RT Polymerase Chain Reaction (qRT-PCR)
  - Intracellular Flow Cytometry for NKX2-1 and SOX2
  - Immunofluorescence Microscopy of Cultured Cells
  - Directed Differentiation of mESCs to Nkx2-1+ Lung Epithelium
  - Forskolin-Induced Swelling of Organoids
- QUANTIFICATION AND STATISTICAL ANALYSIS
  - Statistical Methods
- DATA AND SOFTWARE AVAILABILITY
- ADDITIONAL RESOURCES

SUPPLEMENTAL INFORMATION

Supplemental Information includes six figures, three tables, and three movies and can be found with this article online at http://dx.doi.org/10.1016/j.stem.2017.03.001.

AUTHOR CONTRIBUTIONS

K.B.M. and D.N.K. designed the project, developed experiments, analyzed data, and wrote the manuscript. K.B.M. performed the experiments. F.H., M.S., A.J., and D.C.T. designed and performed additional experiments and analyzed data.

ACKNOWLEDGMENTS

We thank members of the Kotton-Wilson-Ikonomou laboratory for helpful discussions and manuscript review. We thank Aleksander Szymaniak, Julia Berthet, and Anne Hinds for assistance with histology methods and Nicholas Skvir for microarray analysis. We are grateful to Brian Tilton of the Boston University Flow Cytometry Core, supported by grant 1UL1TR001430, and Drs. Greg

Miller and Marianne James of the CReM, supported by NIH grants R24HL123828 and U01TR001810. This work was supported by NIH grant awards F31HL129777-01 (to K.B.M.), F31HL134274-01 and TL1TR001410 (to A.J.), and R01HL122442, R01HL095993, R01HL128172, U01HL099997, U01HL134745, and U01HL134766 (to D.N.K.); awards from the Cystic Fibrosis Foundation (CFF HAWKIN15XX0 to F.H. and CFF DAVIS15XX1 to D.N.K.), and an award from the Massachusetts Life Sciences Center to the CReM.

Received: November 2, 2016
Revised: January 16, 2017
Accepted: March 3, 2017
Published: March 30, 2017

REFERENCES

Bellusci, S., Grindley, J., Emoto, H., Itoh, N., and Hogan, B. (1997). Fibroblast growth factor 10 (FGF10) and branching morphogenesis in the embryonic mouse lung. Development *124*, 4867–4878.

Bilodeau, M., Shojaie, S., Ackerley, C., Post, M., and Rossant, J. (2014). Identification of a proximal progenitor population from murine fetal lungs with clonogenic and multilineage differentiation potential. Stem Cell Reports *3*, 634–649.

Cardoso, W.V., Itoh, A., Nogawa, H., Mason, I., and Brody, J.S. (1997). FGF-1 and FGF-7 induce distinct patterns of growth and differentiation in embryonic lung epithelium. Dev. Dyn. *208*, 398–405.

Chen, F., Desai, T.J., Qian, J., Niederreither, K., Lü, J., and Cardoso, W.V. (2007). Inhibition of Tgf beta signaling by endogenous retinoic acid is essential for primary lung bud induction. Development *134*, 2969–2979.

Chen, F., Cao, Y., Qian, J., Shao, F., Niederreither, K., and Cardoso, W.V. (2010). A retinoic acid-dependent network in the foregut controls formation of the mouse lung primordium. J. Clin. Invest. *120*, 2040–2048.

Crane, A.M., Kramer, P., Bui, J.H., Chung, W.J., Li, X.S., Gonzalez-Garay, M.L., Hawkins, F., Liao, W., Mora, D., Choi, S., et al. (2015). Targeted correction and restored function of the CFTR gene in cystic fibrosis induced pluripotent stem cells. Stem Cell Reports *4*, 569–577.

De Langhe, S.P., Sala, F.G., Del Moral, P.-M., Fairbanks, T.J., Yamada, K.M., Warburton, D., Burns, R.C., and Bellusci, S. (2005). Dickkopf-1 (DKK1) reveals that fibronectin is a major target of Wnt signaling in branching morphogenesis of the mouse embryonic lung. Dev. Biol. *277*, 316–331.

Dekkers, J.F., Wiegerinck, C.L., de Jonge, H.R., Bronsveld, I., Janssens, H.M., de Winter-de Groot, K.M., Brandsma, A.M., de Jong, N.W.M., Bijvelds, M.J.C., Scholte, B.J., et al. (2013). A functional CFTR assay using primary cystic fibrosis intestinal organoids. Nat. Med. *19*, 939–945.

Dye, B.R., Hill, D.R., Ferguson, M.A., Tsai, Y.H., Nagy, M.S., Dyal, R., Wells, J.M., Mayhew, C.N., Nattiv, R., Klein, O.D., et al. (2015). In vitro generation of human pluripotent stem cell derived lung organoids. eLife *4*, e05098.

Firth, A.L., Dargitz, C.T., Qualls, S.J., Menon, T., Wright, R., Singer, O., Gage, F.H., Khanna, A., and Verma, I.M. (2014). Generation of multiciliated cells in functional airway epithelia from human induced pluripotent stem cells. Proc. Natl. Acad. Sci. USA *111*, E1723–E1730.

Fuerer, C., and Nusse, R. (2010). Lentiviral vectors to probe and manipulate the Wnt signaling pathway. PLoS ONE *5*, e9370.

Goss, A.M., Tian, Y., Tsukiyama, T., Cohen, E.D., Zhou, D., Lu, M.M., Yamaguchi, T.P., and Morrisey, E.E. (2009). Wnt2/2b and beta-catenin signaling are necessary and sufficient to specify lung progenitors in the foregut. Dev. Cell *17*, 290–298.

Gotoh, S., Ito, I., Nagasaki, T., Yamamoto, Y., Konishi, S., Korogi, Y., Matsumoto, H., Muro, S., Hirai, T., Funato, M., et al. (2014). Generation of alveolar epithelial spheroids via isolated progenitor cells from human pluripotent stem cells. Stem Cell Reports *3*, 394–403.

Green, M.D., Chen, A., Nostro, M.-C., d'Souza, S.L., Schaniel, C., Lemischka, I.R., Gouon-Evans, V., Keller, G., and Snoeck, H.-W. (2011). Generation of anterior foregut endoderm from human embryonic and induced pluripotent stem cells. Nat. Biotechnol. *29*, 267–272.

Harris-Johnson, K.S., Domyan, E.T., Vezina, C.M., and Sun, X. (2009). beta-Catenin promotes respiratory progenitor identity in mouse foregut. Proc. Natl. Acad. Sci. USA *106*, 16287–16292.

Hashimoto, S., Chen, H., Que, J., Brockway, B.L., Drake, J.A., Snyder, J.C., Randell, S.H., and Stripp, B.R. (2012). β-Catenin-SOX2 signaling regulates the fate of developing airway epithelium. J. Cell Sci. *125*, 932–942.

Hawkins, F., Kramer, P., Jacob, A., Driver, I., Thomas, D.C., McCauley, K.B., Skvir, N., Crane, A.M., Kurmann, A.A., Hollenberg, A.N., et al. (2017). Prospective isolation of NKX2-1-expressing human lung progenitors derived from pluripotent stem cells. J. Clin. Invest. Published online May 2, 2017. http://dx.doi.org/10.1172/JCI89950.

Huang, S.X.L., Islam, M.N., O'Neill, J., Hu, Z., Yang, Y.-G., Chen, Y.-W., Mumau, M., Green, M.D., Vunjak-Novakovic, G., Bhattacharya, J., and Snoeck, H.-W. (2014). Efficient generation of lung and airway epithelial cells from human pluripotent stem cells. Nat. Biotechnol. *32*, 84–91.

Huang, S.X.L., Green, M.D., de Carvalho, A.T., Mumau, M., Chen, Y.-W., D'Souza, S.L., and Snoeck, H.-W. (2015). The in vitro generation of lung and airway progenitor cells from human pluripotent stem cells. Nat. Protoc. *10*, 413–425.

Hyatt, B.A., Shangguan, X., and Shannon, J.M. (2004). FGF-10 induces SP-C and Bmp4 and regulates proximal-distal patterning in embryonic tracheal epithelium. Am. J. Physiol. Lung Cell. Mol. Physiol. *287*, L1116–L1126.

Ikeda, K., Clark, J.C., Shaw-White, J.R., Stahlman, M.T., Boutell, C.J., and Whitsett, J.A. (1995). Gene structure and expression of human thyroid transcription factor-1 in respiratory epithelial cells. J. Biol. Chem. *270*, 8108–8114.

Kim, B.R., Van de Laar, E., Cabanero, M., Tarumi, S., Hasenoeder, S., Wang, D., Virtanen, C., Suzuki, T., Bandarchi, B., Sakashita, S., et al. (2016). SOX2 and PI3K cooperate to induce and stabilize a squamous-committed stem cell injury state during lung squamous cell carcinoma pathogenesis. PLoS Biol. *14*, e1002581.

Konishi, S., Gotoh, S., Tateishi, K., Yamamoto, Y., Korogi, Y., Nagasaki, T., Matsumoto, H., Muro, S., Hirai, T., Ito, I., et al. (2016). Directed induction of functional multi-ciliated cells in proximal airway epithelial spheroids from human pluripotent stem cells. Stem Cell Reports *6*, 18–25.

Kurmann, A.A., Serra, M., Hawkins, F., Rankin, S.A., Mori, M., Astapova, I., Ullas, S., Lin, S., Bilodeau, M., Rossant, J., et al. (2015). Regeneration of thyroid function by transplantation of differentiated pluripotent stem cells. Cell Stem Cell *17*, 527–542.

Li, C., Li, A., Li, M., Xing, Y., Chen, H., Hu, L., Tiozzo, C., Anderson, S., Taketo, M.M., and Minoo, P. (2009). Stabilized beta-catenin in lung epithelial cells changes cell fate and leads to tracheal and bronchial polyposis. Dev. Biol. *334*, 97–108.

Liu, Y., and Hogan, B.L.M. (2002). Differential gene expression in the distal tip endoderm of the embryonic mouse lung. Gene Expr. Patterns *2*, 229–233.

Liu, Y., Jiang, H., Crawford, H.C., and Hogan, B.L.M. (2003). Role for ETS domain transcription factors Pea3/Erm in mouse lung development. Dev. Biol. *261*, 10–24.

Longmire, T.A., Ikonomou, L., Hawkins, F., Christodoulou, C., Cao, Y., Jean, J.C., Kwok, L.W., Mou, H., Rajagopal, J., Shen, S.S., et al. (2012). Efficient derivation of purified lung and thyroid progenitors from embryonic stem cells. Cell Stem Cell *10*, 398–411.

Mootha, V.K., Lindgren, C.M., Eriksson, K.-F., Subramanian, A., Sihag, S., Lehar, J., Puigserver, P., Carlsson, E., Ridderstråle, M., Laurila, E., et al. (2003). PGC-1alpha-responsive genes involved in oxidative phosphorylation are coordinately downregulated in human diabetes. Nat. Genet. *34*, 267–273.

Mou, H., Zhao, R., Sherwood, R., Ahfeldt, T., Lapey, A., Wain, J., Sicilian, L., Izvolsky, K., Musunuru, K., Cowan, C., and Rajagopal, J. (2012). Generation of multipotent lung and airway progenitors from mouse ESCs and patient-specific cystic fibrosis iPSCs. Cell Stem Cell *10*, 385–397.

Mou, H., Vinarsky, V., Tata, P.R., Brazauskas, K., Choi, S.H., Crooke, A.K., Zhang, B., Solomon, G.M., Turner, B., Bihler, H., et al. (2016). Dual SMAD signaling inhibition enables long-term expansion of diverse epithelial basal cells. Cell Stem Cell *19*, 217–231.

Mucenski, M.L., Wert, S.E., Nation, J.M., Loudy, D.E., Huelsken, J., Birchmeier, W., Morrisey, E.E., and Whitsett, J.A. (2003). beta-Catenin is required for specification of proximal/distal cell fate during lung morphogenesis. J. Biol. Chem. *278*, 40231–40238.

Okubo, T., and Hogan, B.L.M. (2004). Hyperactive Wnt signaling changes the developmental potential of embryonic lung endoderm. J. Biol. *3*, 11.

Phelps, D.S., and Floros, J. (1988). Localization of surfactant protein synthesis in human lung by in situ hybridization. Am. Rev. Respir. Dis. *137*, 939–942.

Ramasamy, S.K., Mailleux, A.A., Gupte, V.V., Mata, F., Sala, F.G., Veltmaat, J.M., Del Moral, P.M., De Langhe, S., Parsa, S., Kelly, L.K., et al. (2007). Fgf10 dosage is critical for the amplification of epithelial cell progenitors and for the formation of multiple mesenchymal lineages during lung development. Dev. Biol. *307*, 237–247.

Rawlins, E.L., Clark, C.P., Xue, Y., and Hogan, B.L.M. (2009). The Id2+ distal tip lung epithelium contains individual multipotent embryonic progenitor cells. Development *136*, 3741–3745.

Reynolds, S.D., Zemke, A.C., Giangreco, A., Brockway, B.L., Teisanu, R.M., Drake, J.A., Mariani, T., Di, P.Y., Taketo, M.M., and Stripp, B.R. (2008). Conditional stabilization of β-catenin expands the pool of lung stem cells. Stem Cells *26*, 1337–1346.

Rock, J.R., Onaitis, M.W., Rawlins, E.L., Lu, Y., Clark, C.P., Xue, Y., Randell, S.H., and Hogan, B.L.M. (2009). Basal cells as stem cells of the mouse trachea and human airway epithelium. Proc. Natl. Acad. Sci. USA *106*, 12771–12775.

Sekine, K., Ohuchi, H., Fujiwara, M., Yamasaki, M., Yoshizawa, T., Sato, T., Yagishita, N., Matsui, D., Koga, Y., Itoh, N., and Kato, S. (1999). Fgf10 is essential for limb and lung formation. Nat. Genet. *21*, 138–141.

Shu, W., Guttentag, S., Wang, Z., Andl, T., Ballard, P., Lu, M.M., Piccolo, S., Birchmeier, W., Whitsett, J.A., Millar, S.E., and Morrisey, E.E. (2005). Wnt/beta-catenin signaling acts upstream of N-myc, BMP4, and FGF signaling to regulate proximal-distal patterning in the lung. Dev. Biol. *283*, 226–239.

Somers, A., Jean, J.-C., Sommer, C.A., Omari, A., Ford, C.C., Mills, J.A., Ying, L., Sommer, A.G., Jean, J.M., Smith, B.W., et al. (2010). Generation of transgene-free lung disease-specific human induced pluripotent stem cells using a single excisable lentiviral stem cell cassette. Stem Cells *28*, 1728–1740.

ten Berge, D., Koole, W., Fuerer, C., Fish, M., Eroglu, E., and Nusse, R. (2008). Wnt signaling mediates self-organization and axis formation in embryoid bodies. Cell Stem Cell *3*, 508–518.

Tsao, P.N., Vasconcelos, M., Izvolsky, K.I., Qian, J., Lu, J., and Cardoso, W.V. (2009). Notch signaling controls the balance of ciliated and secretory cell fates in developing airways. Development *136*, 2297–2307.

Volckaert, T., Campbell, A., Dill, E., Li, C., Minoo, P., and De Langhe, S. (2013). Localized Fgf10 expression is not required for lung branching morphogenesis but prevents differentiation of epithelial progenitors. Development *140*, 3731–3742.

Wang, R., Ahmed, J., Wang, G., Hassan, I., Strulovici-Barel, Y., Hackett, N.R., and Crystal, R.G. (2011). Down-regulation of the canonical Wnt β-catenin pathway in the airway epithelium of healthy smokers and smokers with COPD. PLoS ONE *6*, e14793.

Weaver, M., Yingling, J.M., Dunn, N.R., Bellusci, S., and Hogan, B.L. (1999). Bmp signaling regulates proximal-distal differentiation of endoderm in mouse lung development. Development *126*, 4005–4015.

Weaver, M., Dunn, N.R., and Hogan, B.L. (2000). Bmp4 and Fgf10 play opposing roles during lung bud morphogenesis. Development *127*, 2695–2704.

Wilson, A.A., Murphy, G.J., Hamakawa, H., Kwok, L.W., Srinivasan, S., Hovav, A.-H., Mulligan, R.C., Amar, S., Suki, B., and Kotton, D.N. (2010). Amelioration of emphysema in mice through lentiviral transduction of long-lived pulmonary alveolar macrophages. J. Clin. Invest. *120*, 379–389.

Wong, A.P., Bear, C.E., Chin, S., Pasceri, P., Thompson, T.O., Huan, L.-J., Ratjen, F., Ellis, J., and Rossant, J. (2012). Directed differentiation of human pluripotent stem cells into mature airway epithelia expressing functional CFTR protein. Nat. Biotechnol. *30*, 876–882.

Xu, Y., Mizuno, T., Sridharan, A., Du, Y., Guo, M., Tang, J., Wikenheiser-Brokamp, K.A., Perl, A.T., Funari, V.A., Gokey, J.J., et al. (2016). Single-cell RNA sequencing identifies diverse roles of epithelial cells in idiopathic pulmonary fibrosis. JCI Insight *1*, e90558.

You, Y., Richer, E.J., Huang, T., and Brody, S.L. (2002). Growth and differentiation of mouse tracheal epithelial cells: selection of a proliferative population. Am. J. Physiol. Lung Cell. Mol. Physiol. *283*, L1315–L1321.

Zemke, A.C., Teisanu, R.M., Giangreco, A., Drake, J.A., Brockway, B.L., Reynolds, S.D., and Stripp, B.R. (2009). beta-Catenin is not necessary for maintenance or repair of the bronchiolar epithelium. Am. J. Respir. Cell Mol. Biol. *41*, 535–5430.

STAR★METHODS

KEY RESOURCES TABLE

REAGENT or RESOURCE	SOURCE	IDENTIFIER
Antibodies		
Rabbit monoclonal to NKX2-1 (clone EP15847)	Abcam	Cat.# ab76013
Mouse monoclonal to NKX2-1 (clone 8G7G3/1)	Abcam	Cat.# ab72876
Mouse monoclonal to FOXA2 (clone HNF-3B)	Santa Crus	Cat.# sc-101060
Mouse monoclonal to SOX2 (clone O30-678)	BD Biosciences	Cat.# 561469
Goat polyclonal to SOX2	Santa Cruz	Cat.# sc-17320
Mouse monoclonal to TP63 (clone 4A4)	BioCare Medical	Cat.# 163
Rabbit polyclonal to TP63	Santa Cruz	Cat.# sc-8344
Chicken polyclonal to KRT5	Biolegend	Cat.# 905901
Mouse monoclonal to EPCAM (clone AUA1)	Abcam	Cat.# ab20160
Rabbit polyclonal to Pro-SPB	Seven Hills	Cat.# WRAB-55522
Rabbit monoclonal to SCGB3A2 (clone EPR11463)	Abcam	Cat.#. ab181853
Mouse monoclonal to MUC5AC (clone 45M1)	ThermoFisher	Cat.# MA1-38223
Rabbit monoclonal to acetylated alpha-tubulin (clone D20G3)	Cell Signaling Technologies	Cat.# 5335
Mouse monoclonal to CD26, PE conjugated (clone BA5b)	Biolegend	Cat.# 302705
Mouse monoclonal to CD47, PerCP-Cy5.5 conjugated (clone CC2C6)	Biolegend	Cat.# 323110
AffiniPure Donkey Anti-Rabbit IgG (H+L), 488 conjugated	Jackson Immunoresearch	Cat.# 711-225-152
AffiniPure Donkey Anti-Rabbit IgG (H+L), Cy3 conjugated	Jackson Immunoresearch	Cat.# 711-165-152
AffiniPure Donkey Anti-Rabbit IgG (H+L), AlexaFluor 647 conjugated	Jackson Immunoresearch	Cat.# 711-605-152
AffiniPure Donkey Anti-Mouse IgG (H+L), AlexaFluor 647 conjugated	Jackson Immunoresearch	Cat.# 715-605-150
AffiniPure Donkey Anti-Mouse IgG (H+L), AlexaFluor Cy3 conjugated	Jackson Immunoresearch	Cat.# 715-165-150
AffiniPure Donkey Anti-Goat IgG (H+L), AlexaFluor 647 conjugated	Jackson Immunoresearch	Cat.# 305-605-003
AffiniPure Donkey Anti-Chicken IgG (H+L), AlexaFluor 488 conjugated	Jackson Immunoresearch	Cat.# 703-545-155
Human Cell Surface Marker Screening Panel	BD Biosciences	Cat.# 560747
Chemicals, Peptides, and Recombinant Proteins		
Growth Factor Reduced Matrigel	Corning	Cat.# 356230
SB431542	Tocris	Cat.# 1614
Dorsomorphin	Stemgent	Cat.# 04-0024
CHIR99021	Tocris	Cat.# 4423
Recombinant human FGF10	R&D Systems	Cat.# 345-FG-025
Recombinant human KGF	R&D Systems	Cat.# 251-KG-010
Recombinant human BMP4	R&D Systems	Cat.# 314-BP
Retinoic acid	Sigma	Cat.# R2625
Y-27632 dihydrochloride	Tocris	Cat.# 1254
Recombinant human FGF2	R&D Systems	Cat.# 233-FB
Recombinant human TGFβ	R&D Systems	Cat.# 240-B
DAPT	Sigma	Cat.# D5942
Dexamethasone	Sigma	Cat.# D4902
8-bromoadenosine 3′,5′-cyclic monophosphate sodium salt (cAMP)	Sigma	Cat.# B7880
3-Isobutyl-1-methylxanthine (IBMX)	Sigma	Cat.# I5879
Forskolin	Sigma	Cat.# F3917
AlexaFluor 647 Phalloidin	ThermoFisher Scientific	Cat.# A22287
Hoechst	ThermoFisher Scientific	H3570
Recombinant mouse Noggin	R&D Systems	Cat.# 1967-NG
Recombinant mouse Wnt3a	R&D Systems	Cat.# 1324-WN

(*Continued on next page*)

Continued

REAGENT or RESOURCE	SOURCE	IDENTIFIER
Recombinant human Wnt3a	R&D Systems	Cat.# 5036-WN
Critical Commercial Assays		
RNeasy Mini Kit	QIAGEN	Cat.# 74104
QIAzol Lysis Reagent	QIAGEN	Cat.# 79306
TaqMan Fast Universal PCR Master Mix (2X), no AmpErase UNG	ThermoFisher Scientific	Cat.# 4364103
Deposited Data		
Microarray database of time course of differentiating NKX2-1+ lung epithelium	Hawkins et al., 2017	GEO: GSE83310
Experimental Models: Cell Lines		
Human: Normal donor induced pluripotent stem cell (iPSC) line (BU3)	Kotton Lab (Kurmann et al., 2015)	www.bumc.bu.edu/stemcells
Human: Normal donor iPSC line targeted with NKX2-1^{GFP} (BU3^{GFP})	Kotton Lab (Hawkins et al. 2017).	www.bumc.bu.edu/stemcells
Human: Cystic fibrosis donor iPSC line targeted with NKX2-1^{GFP} (C17)	Gift from Dr. Brian Davis, Houston, TX (Crane et al., 2015)	
Human: Cystic fibrosis donor iPSC line (RC2 204 Δ508/ΔF508)	Kotton Lab (Somers et al., 2010)	www.bumc.bu.edu/stemcells
Human: Corrected cystic fibrosis donor iPSC line (RC2 204 Δ508/WT)	Kotton Lab (Crane et al., 2015)	
Human: Cystic fibrosis donor iPSC line (RC2 202 Δ508/ΔF508)	Kotton Lab (Somers et al., 2010)	www.bumc.bu.edu/stemcells
Human: Corrected cystic fibrosis donor iPSC line (RC2 202 Δ508/WT)	Kotton Lab (Crane et al., 2015).	
Human: RUES2 embryonic stem cell line	Gift from Dr. Ali H. Brivanlou, Rockefeller University	
Mouse: Nkx2-1^{mCherry} embryonic stem cell line	Gift from Dr. Janet Rossant, Hospital for Sick Children, Toronto, Canada (Bilodeau et al., 2014)	
Recombinant DNA		
Ef1alpha-betacatenin(deltaGSK)-SV40-mCherry lentiviral plasmid	Addgene (Gift from Dr. Roel Nusse, Stanford University)	Addgene Plasmid #23412
7xTcf-mCherry lentiviral plasmid	Addgene (Gift from Dr. Roel Nusse, Stanford University)	Addgene Plasmid #24315
pHAGE Ef1alpha-mCherry lentiviral plasmid	this paper	
Sftpc^{GFP} lentiviral plasmid	Kotton Lab (Longmire et al., 2012)	www.kottonlab.com
Sequence-Based Reagents		
TaqMan Gene Expression Assay Primer/Probe Sets	ThermoFisher Scientific	See Table S3 for details per gene
Software and Algorithms		
ImageJ	National Institutes of Health	https://Imagej.nih.gov/ij/
Other		
StemDiff Definitive Endoderm Kit	StemCell Technologies	Cat.# 05110
mTeSR1	StemCell Technologies	Cat.# 05850
PneumaCult ALI Medium	StemCell Technologies	Cat.# 05001
Gentle Cell Dissociation Reagent	StemCell Technologies	Cat.# 07174
ReLeSR	StemCell Technologies	Cat.# 05872
TransIT Transfection Reagent	Mirus Bio	Cat. # Mir2700

CONTACT FOR REAGENT AND RESOURCE SHARING

Further information and requests for reagents may be directed to, and will be fulfilled by, the Lead Contact, Darrell Kotton (dkotton@bu.edu).

EXPERIMENTAL MODEL AND SUBJECT DETAILS

Human ESC/iPSC Reporter Line Generation and Maintenance

The differentiation of iPSC lines was performed under the approval of the Institutional Review Board of Boston University (protocols H27636, H32506, and H33122) and with documented informed consent of all donors. The NKX2-1^{GFP} iPSC lines ("BU3" and "C17")

were derived from a normal donor and an individual with cystic fibrosis carrying a published compound heterozygous CFTR genotype (Crane et al., 2015), respectively. Both lines were targeted with an NKX2-1^{GFP} fluorescent reporter using CRISPR and TALENs technologies, respectively, in previous studies (Hawkins et al., 2017). Two CFTR mutant iPSC lines of genotype ΔF508/ΔF508 (clones RC2 202 and RC2 204; generated from two individual donors with cystic fibrosis) (Somers et al., 2010) and their gene-edited subclones, engineered to each carry one corrected CFTR allele, were obtained from the iPSC Core of the CReM of Boston University and Boston Medical Center (Crane et al., 2015). The RUES2 human embryonic stem cell line was a generous gift from Dr. Ali H. Brivanlou of The Rockefeller University. All human PSC lines were maintained in feeder-free culture conditions in 6-well tissue culture dishes (Corning, Corning, NY) on growth factor reduced Matrigel (Corning) in mTeSR1 medium (Stem Cell Technologies, Vancouver, Canada) by passaging with ReLeSR (Stem Cell Technologies) and Gentle Cell Dissociation Reagent (Stem Cell Technologies). All human ESC/iPSC lines used were characterized for pluripotency and were found to be karyotypically normal. Further details of iPSC derivation, characterization, and culture are available for free download at http://www.bu.edu/dbin/stemcells/protocols.php.

Mouse ESC Reporter Line Maintenance

Nkx2-1^{mCherry} mESCs (Bilodeau et al., 2014) were maintained on inactivated mouse embryonic fibroblasts in DMEM supplemented with 15% FBS, L-glut, LIF, and BME (Kurmann et al., 2015; Longmire et al., 2012). Undifferentiated cells were passaged routinely by single cell dissociation using trypsin, enzyme inactivation, and centrifugation at 300xg for 5 min at 4°C and replated onto previously prepared feeder layers on gelatin-coated plastic.

METHOD DETAILS

Directed Differentiation of hPSCs

NKX2-1+ lung progenitors were generated from hPSCs first by inducing definitive endoderm with STEMdiff Definitive Endoderm Kit (Stem Cell Technologies) for 72 hr (day 0 – 72 hr; this differs from the numbering convention used by the manufacturer's protocol, which describes this period as day 1 – day 4). Endoderm-stage cells were dissociated and passaged in small clumps to growth factor reduced Matrigel-coated (Corning) tissue culture plates (Corning) in base media of IMDM (ThermoFisher, Waltham, MA) and Ham's F12 (ThermoFisher) with B27 Supplement with retinoic acid (Invitrogen, Waltham, MA), N2 Supplement (Invitrogen), 0.1% bovine serum albumin Fraction V (Invitrogen), monothioglycerol (Sigma, St. Louis, MO), Glutamax (ThermoFisher), ascorbic acid (Sigma), and primocin (complete serum free differentiation medium, cSFDM (Kurmann et al., 2015; Longmire et al., 2012)) containing 10 μM SB431542 (Tocris, Bristol, United Kingdom) and 2 μM Dorsomorphin (Stemgent, Lexington, MA) for 72 hr (72 hr – 144 hr) to pattern cells toward anterior foregut endoderm. Cells were then cultured for 9-11 additional days (typically, 144 hr - day 15) in cSFDM containing 3 μM CHIR99021 (Tocris), 10 ng/mL recombinant human FGF10 (rhFGF10, R&D Systems, Minneapolis, MN), 10 ng/mL recombinant human KGF (rhKGF, R&D Systems), 10 ng/mL recombinant human BMP4 (rhBMP4, R&D Systems), and 50 nM retinoid acid (RA, Sigma) or with CHIR, BMP4, and RA alone (for organoid immunostaining), to induce a lung epithelial progenitor fate. Doses of growth factors were determined based on previously published directed differentiation protocols (Huang et al., 2014; Kurmann et al., 2015; Longmire et al., 2012). Lung epithelial specification was evaluated at day 15 of differentiation by flow cytometry for NKX2.1^{GFP} expression, expression of surrogate cell surface markers CD47^{hi}/CD26-, or nuclear NKX2-1 protein content. Surface marker expression was evaluated at this stage of differentiation using a human cell surface marker screening panel (BD Biosciences, San Jose, CA). This protocol is based on previously described approaches (Hawkins et al., 2017; Huang et al., 2014; Longmire et al., 2012).

Neuroectodermal NKX2-1^{GFP+} cells were generated using STEMDdiff Neural Induction Medium (Stem Cell Technologies) according to the manufacturer's protocol with additional puromorphamine (Stemgent, 2 uM) supplementation from Day 6 to Day 12-15. NKX2-1^{GFP+} cells were purified by cell sorting at Day 12-15 (Hawkins et al., 2017).

Purification of NKX2-1+ Lung Progenitors by Cell Sorting

Cells grown in two-dimensional culture were harvested by incubation with 0.05% Trypsin-EDTA for 10-20 min at 37°C. Cells cultured in three-dimensional growth factor reduced Matrigel were harvested by incubation with 2 mg/mL dispase (ThermoFisher) for 30-60 min at 37°C then subsequent incubation with 0.05% trypsin at 37°C until a single cell suspension was achieved. Cells were washed with media containing 10% fetal bovine serum (FBS, ThermoFisher.) Harvested cells were spun at 300 RCF for 5 min at 4°C and resuspended in buffer containing Hank's Balanced Salt Solution (ThermoFisher), 2% FBS and 10 μM Y-27632 (Tocris) and stained with propidium iodide (ThermoFisher) or calcein blue AM (ThermoFisher) for dead cell exclusion during flow cytometry. Live cells were sorted on a high speed cell sorter (MoFlo Legacy, Beckman Coulter, Pasadena, CA) at the Boston University Medical Center Flow Cytometry Core Facility based on NKX2-1^{GFP} expression or by staining for CD47 (Biolegend) and CD26 (Biolegend) and gating for CD47^{hi}/CD26^{-}. Although nearly 100% of all differentiated cells are CD47+ at day 15 of directed differentiation, isolating cells in the region of the CD47 cloud brighter than the CD26+ population (CD47^{hi}, representative gate depicted in Figure S5A) results in significant enrichment of the NKX2-1+ lung progenitor population (Figures 6B and S5A) (Hawkins et al., 2017).

Post-Specification Patterning of Lung Epithelial Progenitors

Day 14-16 cells from the lung progenitor directed differentiation protocol were harvested with 0.05% Trypsin-EDTA (Invitrogen) and replated in small clumps to improve survival (for unsorted experiments) or after single cell sorting in either growth factor reduced

Matrigel-coated tissue culture dishes in two-dimensional culture (unsorted clumps only) or in three-dimensional growth factor reduced Matrigel drops (both unsorted clumps and sorted single cells).

Matrigel drops were formed by resuspending cells directly in undiluted growth factor reduced Matrigel matrix, pipetting 50-100 μL into each well, and allowing the Matrigel / cell mixture to gel for 30 min at 37°C. Cell drops were then covered completely with growth medium.

Post-specification culture conditions were determined by the addition of growth factors to cSFDM. For patterning experiments, growth factors were added to a base media containing 10 ng/mL rhFGF10 (“Base”) and additional factors detailed in the results text. For concentrations of growth factors required for each experiment, see Table S2. Doses of growth factors were determined based on previously published directed differentiation protocols (Huang et al., 2014; Kurmann et al., 2015; Longmire et al., 2012) as well as dose-response experiments using 7XTCF lentiviral reporters for CHIR99021 (Figures S2D and S2E). Cells were additionally cultured with 10 μM Y-27632 (Tocris) for 24 hr after replating.

The final protocol for generating rapidly proximalized NKX2-1+ lung epithelium was replating unsorted or sorted cells for 4 days of culture post-specification in cSFDM containing 10 ng/mL FGF10. Sorted cells were cultured with additional factors: 50 nM dexamethasone (Sigma), 0.1 mM 8-Bromoadenosine 3′,5′-cyclic monophosphate sodium salt (Sigma) and 0.1 mM 3-Isobutyl-1-methylxanthine (IBMX) (Sigma) (DCI), and Y-27632. Cells were analyzed for expression of proximal markers 4 days post-replating in FGF10 media.

For organoid experiments, cells were cultured in “CFK media” containing 3 μM CHIR99021, 10 ng/mL rhFGF10, and 10 ng/mL rhKGF or “2+10 media” containing 250 ng/mL recombinant human FGF2 (rhFGF2, R&D Systems) and 100 ng/mL rhFGF10. We further supplemented these medias with DCI and Y-27632. All organoid formation experiments were performed on replated purified, single cell lung progenitors.

Therefore, in the final protocol for the generation of proximalized organoids, single sorted NKX2-1+ cells were replated as 50,000-100,000 cells per well cultured in cSFDM with FGF2 (250 ng/mL), FGF10 (100 ng/mL), DCI, and Y-27632 for at least one week post-sort prior to analysis. Proximalized organoids were maintained for up to 6 weeks after sorting, with media changed every other day. Ciliation was induced in proximalized organoids by Notch inhibition using DAPT (2 μM, Sigma) in organoids after outgrowth least 2 weeks post-sort. Generation of motile cilia was observed by 2 weeks post-DAPT treatment.

Images of cultured organoids, including videos, were taken on a Keyence (Osaka, Japan) BZ-X700 fluorescence microscope. Z stack images were processed using full focus image analysis using Keyence software.

For formation of ALI cultures, proximalized cells were trypsinized and replated in two-dimensional culture on TransWell inserts (Corning) at a confluency of 100,000 cells/cm^2. Expansion was performed in PneumaCult ALI media (Stem Cell Technologies) containing dexamethasone to replace hydrocortisone with additional SMAD inhibition by Dorsomorphin (2 μM) and SB431542 (10 μM) until confluent (Mou et al., 2016). After expansion of cells to confluence, media was removed from the top chamber and cells were differentiated in PneumaCult ALI media with dexamethasone but without SMAD inhibition. Motile ciliated cells were observed by one week post-induction of ALI differentiation. ALI cultures were characterized by immunofluorescent staining for acetylated alpha tubulin, Hoechst and F-actin (phalloidin, Applied Biosystems) and z stack images were taken on a confocal microscope (Zeiss). Orthogonal and maximum intensity Z-projections were generated using ImageJ.

Gene Set Enrichment Analysis

Gene set enrichment analysis was performed using MSigDB v5.1 hallmark gene sets (http://software.broadinstitute.org/gsea/index.jsp) (Mootha et al., 2003) on our previously described microarray database (Hawkins et al., 2017). All raw data files can be downloaded from the gene expression ombinus, GEO: GSE83310. Significant pathways were considered those with Benjamini-Hochberg false discovery rate-adjusted p value (FDR) < 0.1.

Generation of Lentiviral Reporters for Wnt Signaling

VSV-G pseudotyped lentiviral plasmids for β-catenin overexpression (EF1alpha-betacatenin(deltaGSK)-SV40-mCherry, Addgene Plasmid #23412) (Fuerer and Nusse, 2010) and the canonical Wnt reporter 7xTcf-mCherry (Addgene Plasmid #24315) (ten Berge et al., 2008) were a generous gift from Dr. Roel Nusse (Stanford University, Stanford, CA). Lentiviral particles were packaged in 293T cells using a five-plasmid system (Wilson et al., 2010). Briefly, 293T cells were transfected using Trans-IT Transfection Reagent (Mirus Bio, Madison, WI) with plasmids for a lentiviral backbone (e.g., 7XTCF-mCherry) and lentiviral packaging proteins tat, rev, gag/pol and vsv-g. Supernatants were collected after 48 hr and concentrated by centrifugation at 16.5K RPM for 90 min. To calculate titers of packaged viruses, FG293 cells were transduced with concentrated virus in 10% FBS with polybrene (5 μg/mL) and transduction efficiency was quantified after 72 hr by flow cytometry. For the 7XTCF-mCherry virus, cells were treated for 48 hr of 3 μM CHIR99021 prior to titering by flow cytometry. For each experiment, parallel wells were infected with the same MOI of a pHAGE EF1a-mCherry virus as a control for infection efficiency and nonspecific effects of lentiviral infection.

Reverse Transcriptase Quantitative RT Polymerase Chain Reaction (qRT-PCR)

Measurement of mRNA expression was performed by reverse transcriptase quantitative RT PCR (qRT-PCR). RNA was extracted from cells using a QIAzol Lysis Reagent (QIAGEN, Venlo, Netherlands) and 150 ng of RNA was transcribed to cDNA using reverse transcription reagents (Applied Biosystems). RT PCR (qPCR) was performed using TaqMan Fast Universal PCR Master Mix (ThermoFisher) and TaqMan (Applied Biosystems) reagents. The cDNA was diluted 1:3 and 2 μL of cDNA was added to each

25 μL (for Applied Biosystems StepOne 96-well System) or 12.5 μL (for Applied Biosystems QuantStudio7 384-well system) qPCR reaction. Each sample was run in technical triplicates and cycle (Ct) values were averaged between triplicates for analysis. Relative gene expression, normalized to 18S control, was calculated as fold change in 18S-normalized gene expression, compared to baseline, using the $2^{(-\Delta\Delta CT)}$ method. Baseline, defined as fold change = 1, was set to undifferentiated iPSC levels, or if undetected, a cycle number of 40 was assigned to allow fold change calculations. Adult lung control RNA was extracted from a normal lung biopsy sample. Primers were all TaqMan probes purchased from Applied Biosystems. Specifics of primers used are detailed in Table S3.

Intracellular Flow Cytometry for NKX2-1 and SOX2

Cells were harvested for intracellular flow cytometry and fixed for 10-20 min at 37°C in fresh 1.6% paraformaldehyde. Cells were permeabilized with Cell Permeabilization Buffer (eBioscience, San Diego, CA) containing 4% normal donkey serum (Sigma) in PBS and stained with primary antibody for NKX2-1 (Abcam rabbit, 1:100) or a conjugated antibody for SOX2 (BD Biosciences, 1:100). Anti-NKX2-1 antibody was detected by secondary antibody staining with either Cy3, Alexa Fluor 488, or Alexa Fluor 647 fluorophore-conjugated secondary antibodies (AffiniPure Donkey Anti-Rabbit IgG (H+L); 1:500; Jackson ImmunoResearch, West Grove, PA). Stained cells were analyzed on a FacsCalibur instrument (BD Biosciences) and data were analyzed with FlowJo software (Ashland, OR).

Immunofluorescence Microscopy of Cultured Cells

Cells for immunofluorescence microscopy were cultured on glass coverslips (ThermoFisher). Cultured cells were fixed with fresh 4% paraformaldehyde. Cells were permeabilized with 0.3% Triton-X (Sigma) for 10 min at room temperature then blocked with 4% normal donkey serum (Sigma) for 30 min at room temperature. Cells were incubated with primary antibodies (antibody information and sources are detailed in the Key Resources Table) overnight at 4°C, washed, and incubated with secondary antibodies for 30-60 min at room temperature. All secondary antibodies were conjugated to Alexa Fluor 488, Cy3, or Alexa Fluor 647 (Jackson Immunoresearch, 1:500). After antibody staining, nuclei were stained with Hoechst dye (ThermoFisher, 1:500). Coverslips with cells were mounted on glass slides using Prolong Diamond Anti-Fade Mounting Reagent (ThermoFisher) and imaged on a Nikon (Tokyo, Japan) deconvolution microscope.

Three-dimensional organoids were harvested by incubating for 1 hr with dispase and fixed with fresh 4% paraformaldehyde. Whole organoids were stained as described for cultured cells, with slightly longer permeabilization, blocking wash, and antibody incubation steps. For whole mount imaging, organoids were mounted on cavity slides and visualized with a Zeiss (Jena, Germany) confocal microscope.

Quantification of nuclear colocalization was performed using Nikon NIS Elements software using the Object Count function. 3-5 areas from each slide were analyzed for each replicate. The total image area where NKX2-1 and SOX2, SOX9 or TP63 overlapped was divided by the area containing only the NKX2-1 stain.

Directed Differentiation of mESCs to Nkx2-1+ Lung Epithelium

Nkx2-1^{mCherry} mESCs (Bilodeau et al., 2014) were differentiated to lung epithelium based on our previously published protocol (Longmire et al., 2012). First, LIF was withdrawn for 60 hr to induce embryoid body (EB) formation. EBs were then treated with 100 ng/mL activin A (R&D Systems) for 60 hr. Anterior foregut endoderm was generated by dual BMP4 and TGFβ inhibition by SB431542 (10 μM) and rmNoggin (100 ng/mL, R&D Systems) for 24 hr. Lung specification was induced using rmWnt3a (100 ng/mL) and rmBMP4 (10 ng/mL). Cells were sorted on day 14 for Nkx2-1^{mCherry} expression and replated for 2D culture outgrowth containing rhFGF2 (250 ng/mL) and rhFGF10 (100 ng/mL) as previously published (Kurmann et al., 2015) and rmWnt3a (100 ng/mL), as per experimental conditions. On day 16, cells were infected overnight with a Sftpc^{GFP} lentivirus (Longmire et al., 2012) containing a 3.7kb fragment of the human SPC promoter (generous gift of Dr. Jeffrey A. Whitsett, University of Cincinatti) cloned into the promoter of the pHAGE CMV-GFP-w lentiviral plasmid in the place of the CMV promoter (Wilson et al., 2010) in 5 ug/mL polybrene for quantification on day 30 of Sftpc^{GFP+} cell induction.

Forskolin-Induced Swelling of Organoids

Swelling was induced in organoids at Day 22 – 35 of differentiation. Organoids grown in in three-dimensional Matrigel culture in the absence of cyclic AMP and IBMX were passaged to new droplets in 3 μL growth factor reduced Matrigel at least one day prior to swelling. For swelling analysis, organoids were incubated in media containing 5-10 μM forskolin (Sigma) and 10 μM calcein green (ThermoFisher) for 4 – 24 hr at 37°C and 5% CO2. Whole well images were taken using a Keyence BZ-X700 fluorescence microscope at time of forskolin addition and 24 hr later and stitched using Keyence software. Videos were created by imaging every 15 min for 24 hr. Quantification of swelling area was performed from replicate wells images on the calcein green channel using ImageJ. Total well surface area covered by organoids was calculated based on thresholded images and the total well area of circular organoids (circularity = 0.5-1) were measured. If necessary, organoid edges were smoothed using a Gaussian blur filter prior to thresholding and watershedding. The well area at time = 0 was set to 1. Images were again analyzed at 3 and 24 hr post-forskolin addition and the ratio of the post-swelling area to the original area was calculated. Statistics were calculated from separate wells of organoids, with each value comprising 20-50 individual organoids.

QUANTIFICATION AND STATISTICAL ANALYSIS

Statistical Methods

Statistical methods relevant to each figure are outlined in the figure legend. Briefly, unless indicated otherwise in the figure legend, unpaired, two-tailed Student's t tests were used to compare quantitative analyses comprising two groups of n = 3 or more samples, where each replicate ("n") represents either entirely separate differentiations from the pluripotent stem cell stage or replicates differentiated simultaneously and sorted into separate wells. Further specifics about the replicates used in each experiment are available in the figure legends. In these cases, a Gaussian distribution and equal variance between samples was assumed as the experiments represent a large number of random samples of the measured variable. As we anticipated that biologically relevant differences between conditions would have a large effect size and due to the large technical burden of directed differentiation experiments, we set our sample size threshold to at least 3 replicates to ensure our samples were large enough to perform t tests to compare the populations and observe predicted differences. The p value threshold to determine significance was set at $p = 0.05$. Data for quantitative experiments is typically represented as the mean with error bars representing the standard deviation or standard error of the mean, depending on the experimental approach. These details are available in the figure legends. For analysis of dose escalation experiments, an ordinary one-way ANOVA with post test for linear trend was used to test the linear trend in the mean value at the indicated doses from left to right.

DATA AND SOFTWARE AVAILABILITY

The microarray database of the time course of differentiating NKX2-1+ lung epithelium used to generate the heatmap in Figure 2 was described in Hawkins et al. (2017) and has been deposited in GEO: GSE83310.

ADDITIONAL RESOURCES

Further protocol information for iPSC/ESC culture and directed differentiation and production of lentiviral particles can be found at http://www.bu.edu/dbin/stemcells/protocols.php.